frontiers | Frontiers in Earth Science

TYPE Original Research
PUBLISHED 20 September 2022
DOI 10.3389/feart.2022.994258

OPEN ACCESS

EDITED BY
Ya Ping Wang,
East China Normal University, China

REVIEWED BY
Jianzhong Ge,
East China Normal University, China
Zhanhai Li,
East China Normal University, China

*CORRESPONDENCE
Longhai Zhu,
zhulonghai@ouc.edu.cn

SPECIALTY SECTION
This article was submitted to Geohazards and Georisks, a section of the journal Frontiers in Earth Science

RECEIVED 14 July 2022
ACCEPTED 22 August 2022
PUBLISHED 20 September 2022

CITATION
Xie B, Bao R, Yin D, Zhu L, Hu R, Cai W, Liu T, Lin C and Lu P (2022), The spatio-temporal distribution and transport of suspended sediment in Laizhou Bay: Insights from hydrological and sedimentological investigations. *Front. Earth Sci.* 10:994258. doi: 10.3389/feart.2022.994258

The spatio-temporal distribution and transport of suspended sediment in Laizhou Bay: Insights from hydrological and sedimentological investigations

Bo Xie[1], Rui Bao[2], Dongxiao Yin[3], Longhai Zhu[1,4]*, Rijun Hu[1,4], Weiwei Cai[5], Tao Liu[6], Chaoran Lin[1] and Pengfei Lu[1]

[1]College of Marine Geo-Science, Ocean University of China, Qingdao, China, [2]Frontiers Science Center for Deep Ocean Multispheres and Earth System, Key Laboratory of Marine Chemistry Theory and Technology, Ministry of Education, Ocean University of China, Qingdao, China, [3]Virginia Institute of Marine Science, Gloucester Point, VA, United States, [4]Key Lab of Submarine Geosciences and Prospecting Techniques, Ministry of Education, Qingdao, China, [5]Qingdao Boyan Marine Environment Technology Co., Qingdao, China, [6]School of Geography and Ocean Science, Ministry of Education Key Laboratory for Coast and Island Development, Nanjing University, Nanjing, China

Suspended sediment transport and deposition are crucial physical processes controlling the geomorphological evolution of estuaries and bays. Specially, under the context of worldwide coastal erosion, knowledge of the spatio-temporal distribution of suspended sediment concentration (SSC) and its associated sediment load have become increasingly important for bay management. However, our understanding of the mechanisms of suspended sediment dynamics continues to be hampered by the lack of high-resolution observations. Here, we present a study of the transport mechanisms and controlling factors of suspended sediment over Laizhou Bay. For this, we conducted continuous measurements of SSC, salinity, temperature, and flow velocity at nine stations throughout Laizhou Bay for one 25-h period during each of the spring and moderate tides. Based on these data, residual current, gradient Richardson numbers, and suspended sediment flux were calculated. Our results indicate that a strong current field occurs near the Yellow River mouth, corresponding to the zone with high SSC. The overall diffusion characteristics of suspended sediment are controlled by the tidal current field. Furthermore, our findings suggest that different degrees of stratification occur in the water column, which inhibit the effective vertical diffusion of suspended sediment; Higher water temperature was the main cause of stronger water column stratification of spring tide than moderate tide. Finally, our results reveal that the type of seabed sediment is an important factor controlling SSC by influencing resuspension flux. We conclude that the primary mechanisms controlling suspended sediment transport in Laizhou Bay are advection and tidal pumping, especially advection. Our research provides both a foundational reference for the sediment source-to-sink process from the Yellow River to the sea, as well as guideline implications for coastal engineering construction and channel dredging.

KEYWORDS

suspended sediment, spatio-temporal distribution, transport mechanisms, control factors, laizhou bay

1 Introduction

Quantifying suspended sediment load and understanding the physical mechanisms behind it is an important topic of sediment dynamics in estuarine and bay areas (Allen, 2008; Bianchi and Allison, 2009; Yin et al., 2013). Suspended sediment is a major carrier of heavy metals and organic matter, playing a significant role in environmental pollution (Oliveira et al., 2021). In addition, suspended sediment can strongly affect the primary productivity in the ocean by acting as the major carrier of nutrients, or via attenuating the degree of light penetration in the water column (Vonda et al., 2020). Moreover, cross-shore suspended sediment transport can be tied with beach morphodynamics (Pang et al., 2019). Thus, it is essential to quantify suspended sediment transport and reveal the controlling mechanisms behind it.

Being typically located in coastal regions, bay areas have some of the highest human development (Xu and Xu, 2013). Suspended sediment transport over bays not only affects seabed evolution and coastal erosion (Jillian et al., 2018), but also largely influences the delivery of nutrients and pollutants from the land to the ocean (Wang et al., 2014; Hu et al., 2016; Nour et al., 2022). Different bays have distinct geomorphic and topographic features, hydrodynamic conditions, and sediment types, as well as suspended sediment transport mechanisms (Fang et al., 2000; Tong et al., 2018; Bo Liu et al., 2020). Since the Anthropocene, human activity has largely transformed upstream rivers (Syvitski and Milliman, 2007)), exerting substantial effects on the patterns of suspended sediment transport in bays (Jillian et al., 2018). The Yellow River is well known for its high SSC (Milliman and Meade, 1983). The seasonal variation of sediment and seawater inflow from the Yellow River has an important effect on the suspended sediment transport pattern in Laizhou Bay (Liu et al., 2013). The mouth of the Yellow River is located at the intersection of the central shallow sea basin of the Bohai Sea and Laizhou Bay; further, the sediment transport from the Yellow River into the sea is the main source of sediment in Laizhou Bay (Qin et al., 1985; Liu et al., 2005; Shou et al., 2016; Bo Liu et al., 2020). Recent studies indicate that sediment input from the Yellow River has decreased considerably due to anthropogenic activities (Wu et al., 2017; Fu et al., 2021). High turbidity zones from the Yellow River estuary to the middle of Laizhou Bay are correlated with seabed sediment types. Fine-grained sediment area within the bay tend to cause high turbidity (Wang and Wang, 2005). Although there are abundant observational and numerical studies in parts of Laizhou Bay, especially at the Yellow River mouth, the physical condition of suspended sediment transport in Laizhou Bay as a whole needs further study.

Remote sensing is widely used to study the suspended sediment transport. Wang and Wang (2005) analyzed the transport path of suspended sediment in Laizhou Bay using Landsat imagery. Similarly, Bi et al. (2011) used Moderate Resolution Imaging Spectroradiometer (MODIS) data to study the seasonal changes in suspended sediment transport in the Yellow River. In addition, the sediments from the Yellow River are mainly transported outward along two pathways by combining the measured data (SSC) with MODIS images and ocean current data (Xingmin Liu et al., 2020). However, remote sensing cannot effectively monitor water below the surface layer; the bottom SSC tends to be larger than the surface SSC, especially when the water column is strongly stratified. Thus, continuous and synchronous investigations are important to understand the continuous variation characteristics and overall transport mechanism of suspended sediment in Laizhou Bay.

Previous research on the sediment dynamics of Laizhou Bay have focused more on the southwest and northeast parts of the bay, or on the Yellow River mouth during the summer and winter seasons (Wang and Wang, 2005; Li et al., 2015; Chao Jiang et al., 2017; Bo Liu et al., 2020). At spring, not only has the amount of water and sediment inflow into the Yellow River increased, and water column stratification in the Bohai Sea at April (Su, 2005; Liu and Pan, 2007), which have an impact on the suspended sediment transport. However, the transport patterns of suspended sediment in Laizhou Bay in the spring, which is the transitional period between winter and summer, remain unclear.

In this study, we conducted continuous measurements of SSC, salinity, temperature and flow velocity for one the tidal cycle (25-h period) at nine sampling stations across Laizhou Bay during each of the spring and moderate tides. The objectives of this study are twofold: 1) to explore the characteristics of spatio-temporal variation of SSC in Laizhou Bay during spring, as well as their primary controlling factors, and 2) to reveal the patterns and influencing factors of suspended sediment transport. Our findings shed light on the distribution characteristics and transport mechanisms of suspended sediment in Laizhou Bay in the spring, which can provide baseline knowledge for bay and estuary management.

2 Background of the study area

Laizhou Bay is one of three bays in the Bohai Sea (Figure 1), which is a semi-enclosed inland sea with a total area of about 77,000 km^2, an average water depth of approximately 18 m, shallower water along the coast, and deeper water in the central basin and Bohai Strait (Zhao et al., 2020). The landforms of eastern Laizhou Bay differ greatly from those of western Laizhou Bay. The coast of the eastern uplift area features a large expanse of typical

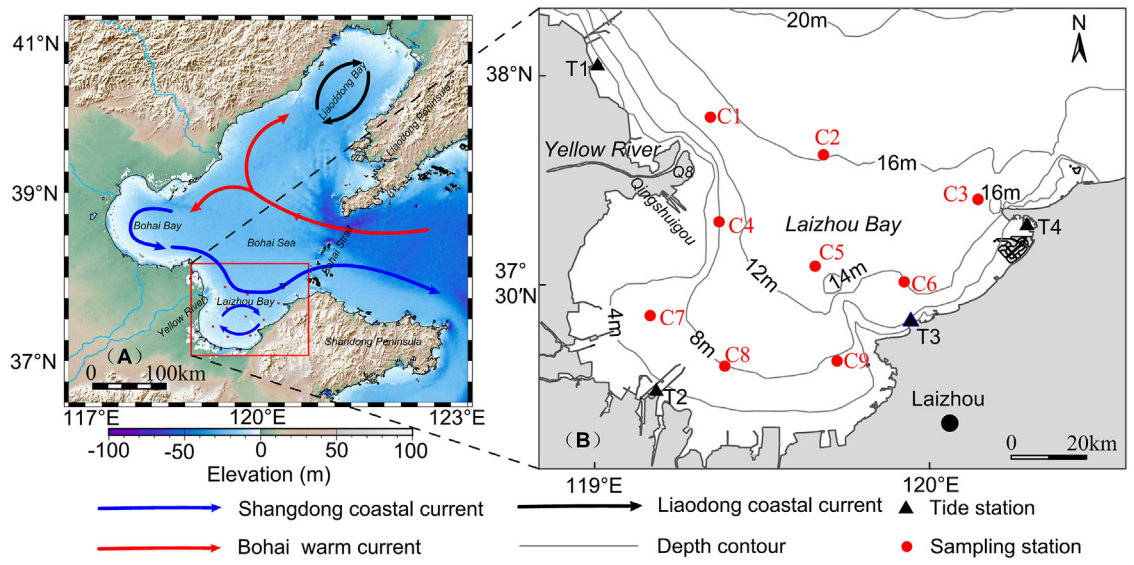

FIGURE 1
(A) Map of the study area (red open box) in the Bohai Sea. The elevation (+) over land and water depth (-) in the ocean are also shown (adapted from Fang et al. (2000)). Blue arrows represent the Shangdong coastal current. Red arrows represent the Bohai warm current. Black arrows represent the Liaodong coastal current **(B)** The red solid circle represents the sampling stations. The black solid triangles represent the tide stations. Gray lines represent isobaths.

sandy coast, mostly lagoons, low hills, sand bars, and sand spits. The topography in the western subsidence area is gentle, with a wide tidal flat, and the seabed sediment types are mainly silt, sandy silt, and silty sand (Zhao et al., 2020). Since the 1950's, the sediment discharge from the Yellow River have experienced stepwise downtrend, decreasing from 1.23 Gt/yr during the period of 1950–1968 to 0.15 Gt/yr during the period of 2000–2005 (Wang et al., 2007).

In terms of hydrodynamics, the tidal range increases as the water depth from the bay mouth to the bay head becomes shallower, with an average water depth of about 10 m, which is a typical shallow bay. The normal wave direction is primarily NE, and the secondary normal wave direction is NNE during winter, with an average wave height of approximately 0.6 m (Qin et al., 1985). The Bohai warm current, Shandong coastal current, and Liaodong coastal current are the main circulation systems in the Bohai Sea during winter, and the circulation does not change its main pattern in spring, in the main studying period of this work (Su, 2005). The circulation flows in from the north and out from the south of the Bohai Strait (Fang et al., 2000) (Figure 1A).

3 Materials and methods

3.1 Materials

The hydrological and sediment data were investigated by two field surveys, each over one tidal cycle (25 h), that included nine sample stations (C1–C9) and four tide stations (T1–T4), conducted in Laizhou Bay during the spring (May 27–28, 2020) and moderate tides (April 24–25, 2020) (Figure 1).

3.1.1 Current and tide

An Acoustic Doppler Current Profiler (ADCP) was mounted in the rear of a ship on the right side, and data were collected every 10 min. The DCX-22–2 Tidal Level Meter (Global Water) and HY1300 Digital Tidal Level Meter (Chengdu CSCC Electronic Technology Co., Ltd.) were used for tidal level observations, with a 1 s sampling interval.

3.1.2 Temperature and salinity

Water temperature (sampling frequency: 5 Hz, accuracy: ±0.005°C) and salinity (sampling frequency: 5 Hz, conductivity measurement accuracy: ±0.009 ms/cm) were measured using a conductivity-temperature-depth (CTD)-NV probe (Teledyne RD Instruments). CTD was devolved at a rate of 0.5 m/s.

3.1.3 Turbidity and SSC

Turbidity was measured using an AQUA logger® 310TY Turbidimeter (Aquatec Group Ltd., Basingstroke, United Kingdom; sampling frequency: 1 Hz, accuracy: ±0.01 NTU). At each station, SSC was measured via filtration weighing at the surface (approximately 1 m from the water surface), middle (0.5 H, H: water depth), and bottom (approximately 1 m from the sea floor) water samples with a volume of about 1,000 ml. SSC was measured by filtration

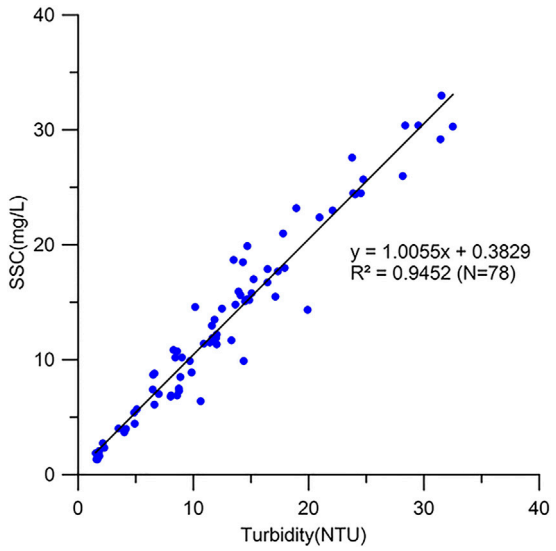

FIGURE 2
The relationship between SSC and turbidity.

weighing. A fiber acetate membrane with a pore size of 0.45 μm was used for extraction, which was then dried and weighed before the data were corrected using a double membrane. SSC was the ratio of sediment bulk density to water sample volume. To verify the accuracy of the SSC measurement, we analyzed the correlation between turbidity and measured SSC at the C2 station (Figure 2); the correlation coefficient was 0.945. Similarly, the correlation coefficient of other stations surpassed 0.82, which indicated that there was a strong corresponding relation between SSC and turbidity (Zhou et al., 2017).

3.2 Methods

3.2.1 Gradient richardson number (*Rig*)

At present, the gradient Richardson number (*Rig*) (Trowbridge, 1992) is one of the most commonly used characteristic parameters for describing the mixing degree (Tong et al., 2018; Meng et al., 2020; Xingmin Liu et al., 2020), and the it is calculated as follows:

$$Rig = -\frac{g}{\rho}\frac{\partial \rho}{\partial z}\left(\frac{\partial u}{\partial z}\right)^{-2} \tag{1}$$

where z denotes the height above the bed and u represents the flow velocity of the corresponding horizon. The *Rig* is compared with the critical value (when *Rig* reached 0.25, stratified mixing is in equilibrium state) to judge the mixing state of the water (Turner and Benton, 1974; Xu and Xu, 2013). When *Rig* was greater than 0.25, the water column was stratified and mixing was inhibited. In contrast, when *Rig* was less than 0.25, the stratification degree weakened and the mixing degree strengthened.

In Eq. 1, ρ is the water density, and can be calculated using the seawater state equation (Millero and Poisson, 1981):

$$\rho = \rho_0 + AS + BS^{3/2} + CS^2 \tag{2}$$

where ρ_0, A, B, and C are functions of water temperature (T), and S is water salinity.

3.2.2 Decomposition of suspended sediment flux

The flux decomposition method proposed was used to calculate suspended sediment transport flux. This method revealed the main contribution rate of different processes by comparing the values of decomposition terms (Dyer, 1997). This method was more mature in domestic and foreign application (Li et al., 2022), but the effect of wave action was not fully considered. This method was more suitable for analyzing seas with weak wave activity. It is known that Laizhou Bay is dominated by monsoon-formed waves and that weak southerly wind prevail at the end of spring (Qin et al., 1985). Therefore, this method was suitable for this research.

In accordance with the method proposed by Ingram (1981) and Uncles et al. (1985) to decompose the instantaneous material flux with relative water depth, the measured velocity (u) was decomposed into $u = \bar{u} + u' = \overline{u_0} + \overline{u_t} + u_0' + u_t'$, where $\overline{u_0}$ and $\overline{u_t}$ represent the mean velocity and oscillatory velocity of $\bar{u}$, respectively; u_0' and u_t' represent the mean velocity and oscillatory velocity of u', respectively. Similarly, SSC (c) were also decomposed, and water depth (h) can be expressed as $h = h_0 + h_t$, where $h_0$and h_t represent the mean depth and oscillatory depth during a tidal cycle. The formula of suspended sediment transport flux (F) in a tidal period (T_t) was calculated using Eq. 3. In this paper, the nomenclature of the parameters in the formulas is following the framework of the Lagrangian transport. Therefore, some parameters may be represented by symbols different from previous studies.

$$\begin{aligned} F &= \frac{1}{T_t}\int_0^{T_t}\int_0^{h} ucdz\,dt \\ &= \underbrace{\frac{h_0\overline{u_0}\overline{c_0}}{T_1}}_{} + \underbrace{\frac{\langle h_t\overline{u_t}\rangle\overline{c_0}}{T_2}}_{} + \underbrace{\frac{\langle h_t\overline{c_t}\rangle\overline{u_0}}{T_3}}_{} + \underbrace{\frac{\langle h_t\overline{u_t c_t}\rangle}{T_4}}_{} + \underbrace{\frac{h_0\overline{u_0'c_0'}}{T_5}}_{} \\ &\quad + \underbrace{\frac{\langle h_t u_0' c_t'\rangle}{T_6}}_{} + \underbrace{\frac{\langle h_t u_t' c_0'\rangle}{T_7}}_{} + \underbrace{\frac{\langle h_t u_t' c_t'\rangle}{T_8}}_{} \end{aligned} \tag{3}$$

where T_1 is the non-tidal flux called the Eulerian flux, T_2 is the Stokes drift flux, and $T_1 + T_2$ is the Lagrange flux, belonging to advection transport term. T_3 is the correlation between tidal and suspended sediment, T_4 is the correlation between suspended sediment and tidal current change, T_5 is the correlation term

between vertical velocity change, and SSC change is the sediment transport term generated by vertical net circulation; $T_3 + T_4 + T_5$ is collectively known as the tidal pumping contribution terms. T_6 is the tidally averaged vertical circulation, T_7 is derived from the change of the vertical distribution of SSC and velocity, and T_8 is the vertical tidal oscillation shear.

First of all, tidal current was decomposed along the *X*-axis (positive direction towards east) and the Y -axis (positive direction towards north). The magnitudes and directions of instantaneous tida1-averaged suspended sediment flux per unit width were computed according to the vector synthesis method.

4 Results

The study area included nine stations that were divided into three groups based on the geographical features in which they were located. Stations C1, C2, and C3 were in the bay mouth; stations C4, C5, and C6 were in the middle of the bay; and stations C7, C8, and C9 were in the head of the bay.

4.1 Variability of SSC

During the spring tide (Figures 3A,B), the horizontal SSC at each station ranged from 1.3 to 18.9 mg/L, and the average SSC was 9.1 mg/L. Overall, compared to SSC in winter, SSC was reduced by 3–4 times due to the large amount of resuspension sediment caused by strong wind in winter (Qiao et al., 2010; Bi et al., 2011). Figure 3A shows that surface SSC varied substantially. SSC levels were found to be high in western Laizhou Bay. The sea at the Yellow River mouth and in southeastern Laizhou Bay likewise showed high-SSC values in this high-SSC zone, but the sea near the abandoned Qingshuigou (QSG) delta had relatively low SSC values. This indicates that the causes of elevated SSC levels in both zones were different. Similarly, satellite remote sensing data revealed the above SSC distribution characteristics (Figure 3E). The surface SSC of the Yellow River mouth decreased rapidly near the shore (no more than 20 km from the mouth). In addition, this surface SSC extended to the southwest nearshore direction. There was a surface low SSC zone in the middle of Laizhou Bay, which is consistent with the previous studies using measured data (Qiao et al., 2010). The average SSC in eastern Laizhou Bay was between that of the west and middle of the bay. The bottom SSC distribution was similar to that of the surface SSC. However, the bottom SSC, located in the area near the Yellow River mouth, had the highest value. During moderate tide, the average SSC (10.1 mg/L) was higher than that of the spring tide (9.1 mg/L), and its coverage was also greater than that of the spring tide. The remaining characteristics were similar to those of the spring tide.

According to the geographical position of the stations, during the spring tide (Figures 4A–I), the SSC at the bay mouth ranged from 1.3 to 30.4 mg/L, with an average SSC of 5.8 mg/L. The SSC at the C1 station near the Yellow River mouth was higher than that at other stations. In the middle of bay, the SSC ranged from 4.8 to 52.5 mg/L, with an average of 8.8 mg/L. The highest SSC value was recorded at the C4 station. At the head of bay, the SSC varied from 4.9 to 57.1 mg/L, and the average SSC reached 14.1 mg/L. The highest SSC zone was recorded at the C7 station. Vertically, the surface SSC was lower than the bottom SSC. For example, the surface SSC at C8 was only 2.4 mg/L, whereas the bottom SSC was 29.2 mg/L. During the moderate tide (Figure 4K–R), the surface SSC ranged between 0.9 and 85.6 mg/L at each station, with an average SSC of 13.4 mg/L. SSC distribution characteristics from the bay mouth to its head were similar to those observed during spring tide, and SSC decreased vertically from surface to bottom. Overall, the SSC in spring was high in western Laizhou Bay and low in eastern Laizhou Bay, high at the head of the bay and low at the bay mouth, and high at the bottom and low at the surface. The average SSC of the spring tide was slightly lower than that of the moderate tide. In the tidal cycle, there were 2–4 times of high SSC field, which generally appeared around the peak of flow velocity; the low SSC field appeared during slack waters period (Figures 4, 6).

4.2 Tidal current and residual current variability

In the study area, the discriminant index (K, K is the ratio of the sum value of the major half axis of the tidal current ellipse of K_1 and O_1 to the value of the major half axis of the tidal current ellipse of M_2) of tidal properties was greater than 0.5 and less than 2, which belonged to the irregular semi-diurnal tidal sea area. Reciprocating current was the main form of tidal current movement, which is consistent with previous studies (Huang et al., 1999). It showed the vertical average tidal current at each station in the spring (Figure 5A) and moderate (Figure 5B) tides. The spring and moderate tide flow directions were similar. The flow direction was essentially the same along the coast, whereas the far coast had rotating current characteristics (Figure 5). In addition to the bay mouth, the terrain gradually widened and began to exhibit a rotating current, and the main direction of flood and ebb tides changed with the coastal trend of the Shandong Peninsula. Furthermore, the flood and ebb tide flow directions were almost symmetric, which was consistent with round-trip flow characteristics. However, the flow direction at the C9 station exhibited some rotating flow features, which were assumed to be produced by the lifting of the convex bank based on the water depth topography (Figure 1). As seen C1 station in Figure 5, there was a high-velocity field in northwestern Laizhou Bay, followed by the middle and eastern Laizhou Bay. This was

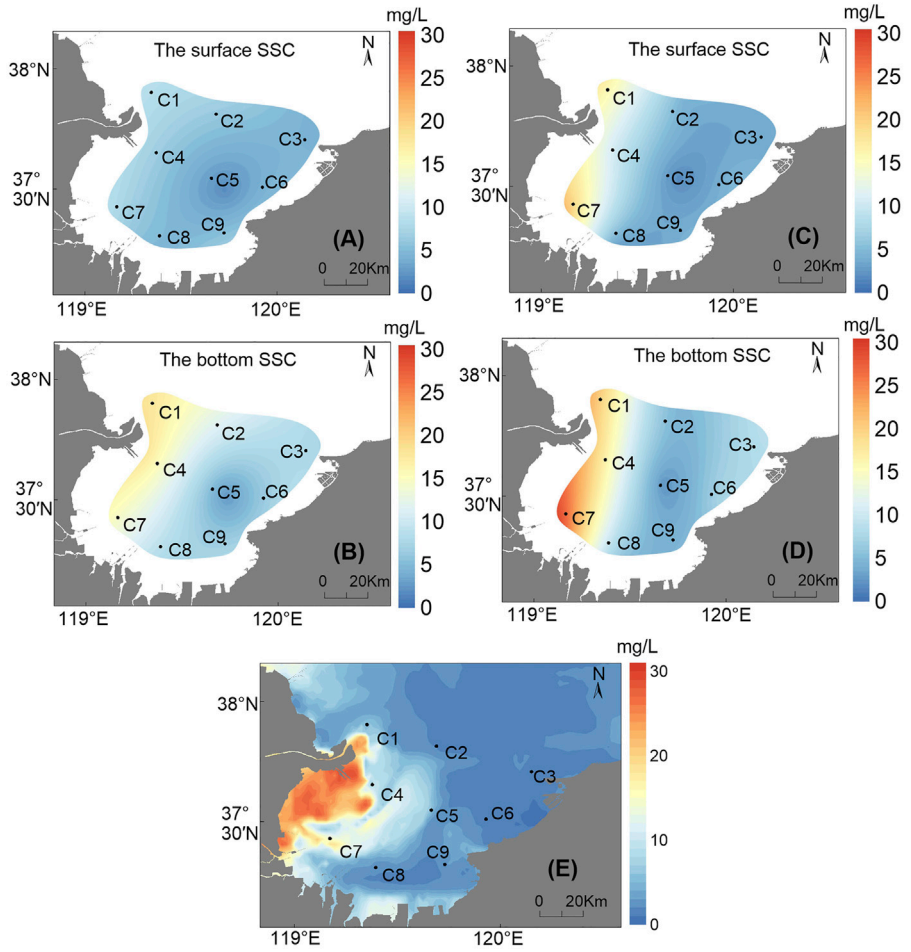

FIGURE 3
Horizontal distribution of the surface SSC **(A)** and the bottom SSC **(B)** during the spring tide (May 24–25, 2020); horizontal distribution of the surface SSC **(C)** and the bottom SSC **(D)** during the moderate tide (April 27–28, 2020). **(E)** Geostationary Ocean Color Imager (GOCI) satellite image of SSC on 23 May 2020.

comparable to the horizontal distribution of SSC analyzed above (Figure 3E).

To further study the distribution characteristics of flow velocity, the vertical flow velocity profiles were analyzed for the spring (Figure 6A) and moderate tides (Figure 6B). There were 3–4 flow velocity peaks in a tidal cycle, which was consistent with characteristics of semi-diurnal tide. These peak values occurred at the flood tide and ebb tide, and the average flow velocity of the flood tide (37.8 cm/s) was slightly higher than that of the ebb tide (37.2 cm/s). Both the spring (93.7 cm/s) and moderate tides (83.0 cm/s) had the highest flow velocity at the C1 station in the area near the Yellow River mouth. The flow velocity decreased gradually from the surface layer to the bottom layer. Furthermore, when the surface flow velocity increased, the bottom flow velocity did increase gradually, albeit with a delay. An asymmetry in the flow velocity and duration between flood and ebb tides was observed during a tidal cycle. In terms of flow velocity, the average flow velocity (36.23 cm/s) of the flood tide was slightly lower than the average flow velocity (40.14 cm/s) of the ebb tide, which might be attributable to topographical influence of the Yellow River Delta (Li, 1990). In addition, flood tide lasted around 1–2 h longer than the ebb tide. Overall, due to the topography of the Yellow River Delta, a strong current field was formed in northwestern Laizhou Bay. There were weak current fields in southeastern Laizhou Bay (Figure 5). The maximum and average surface flow velocity at each station were greater than those at the bottom (Figure 6), and the average ratio of surface flow velocity to bottom flow velocity is 2.65.

Residual current was obtained by separating the periodic tidal current from the measured data. The residual current can indicate the movement and exchange of water (Zhao et al., 1995), which is a critical aspect of further research on suspended sediment transport in shallow continental shelfs. In this study,

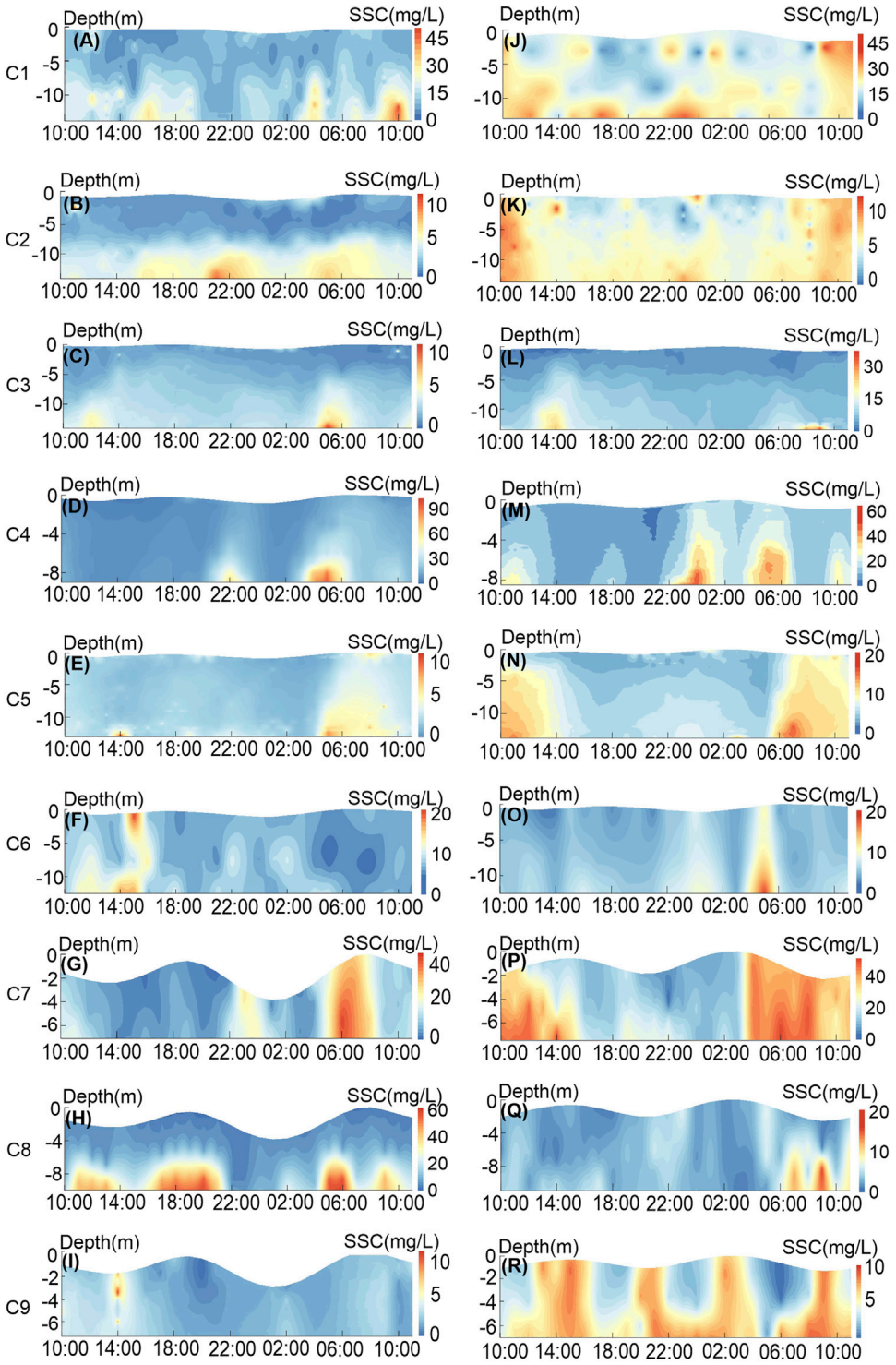

FIGURE 4
Time series of SSC profiles at various stations during the spring **(A–I)** and moderate **(J–R)** tides.

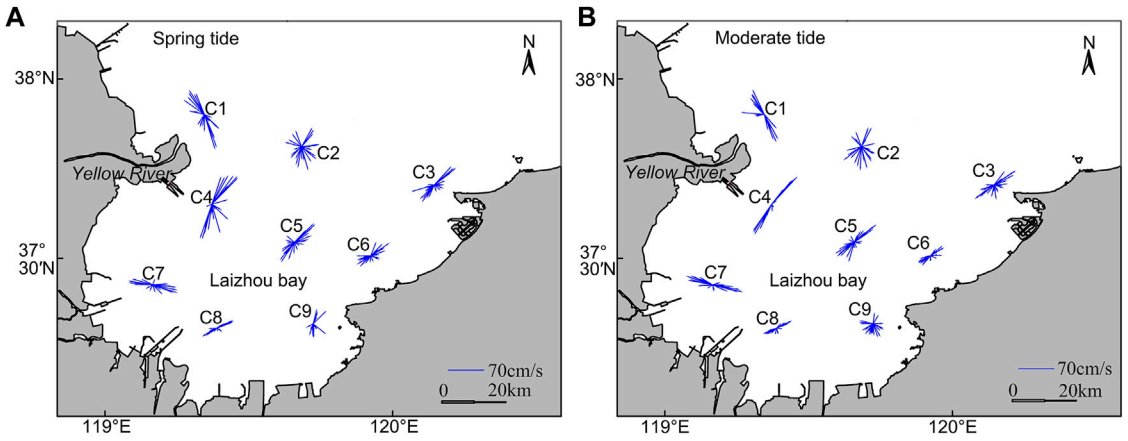

FIGURE 5
Vertical average tidal current at each station during the spring **(A)** and moderate **(B)** tides.

tide-induced residual current was calculated using tidal harmonic analysis through the program 'T_TIDE' package (Table 1). During the spring tide, the residual current velocity in Laizhou Bay ranged between 0.5 and 8.3 cm/s. The C5 station had the lowest bottom residual current velocity, with a flow direction of 151.0°. The surface residual current velocity was the largest at the C3 station, with a flow direction of 91.0°. The residual current velocity was 0.6–10.9 cm/s during the moderate tide period. The bottom residual current velocity was the lowest at the C7 station, and its direction was 231.1°. The C9 station had the greatest bottom residual current velocity. Overall, the residual current velocity was high near the surface and gradually decreased from the surface to the bottom. This was similar to the variation in tidal current velocity. It should be noted that the flow directions of surface and bottom residual currents were not consistent.

4.3 Water temperature and salinity variability

The average temperature increased from the bay mouth to the head of the bay over the whole tidal cycle of the spring and moderate tides (Figures 7A,E). Notably, there was a low salinity zone near southern Laizhou Bay, which may reflect the influence of small local rivers (Qiao et al., 2010). During the spring and moderate tides, surface temperature was generally higher than bottom temperature, while the water salinity variation was the opposite (Figures 7C,D,G,H). The largest water temperature difference was recorded during spring tide at the C1 station in the head of the bay, with a difference of 2.5°C. The maximum salinity difference was 2.0 psu at the C1 station near the Yellow River mouth. In addition, the temperature difference value showed an increasing trend from the head of the bay to the bay mouth (Figures 7B,F), which was similar to the change of water depth. In particular, the increase in solar thermal radiation at noon further increased the temperature difference between surface and bottom water (Simpson and Dickey, 1981). Based on Figures 9A,C,E,G, we found that the average water temperature progressively increased from the mouth to the head of the bay, while the average salinity gradually decreased. Due to the input of other rivers at the head of the bay and the diluted water of the Yellow River (Qiao et al., 2010), the average salinity from the Yellow River mouth to southwestern Laizhou Bay did not exceed 29 psu.

4.4 Mixing degree variability

To better characterize the variation of the water mixing degree in Laizhou Bay, representative stations were selected and *Rig* was used to describe the stratification mixing degree of the water structure. This study set the ordinate to Q ($Q = \mathrm{In}\,(Rig/0.25)$). When Q was greater than 0, the stratification of the water column was high; the greater the value was, the stronger the stratification of the water column was. When Q was less than 0, the vertical mixing degree of the water column increased.

Except for the near bottom, the zone of positive value spanned the bulk of the spring tide (Figures 8A–D), indicating that the stratification degree was high. The C3 station had the largest stratification zone (less than 0), followed by the C4 and C5 stations, and the C9 station had the smallest, which was associated with the low average salinity and shallow water depth of the head of the bay (Chen et al., 2015). The high value zone was mostly concentrated at about 14:00, which is thought to be caused by solar thermal radiation, and the temperature

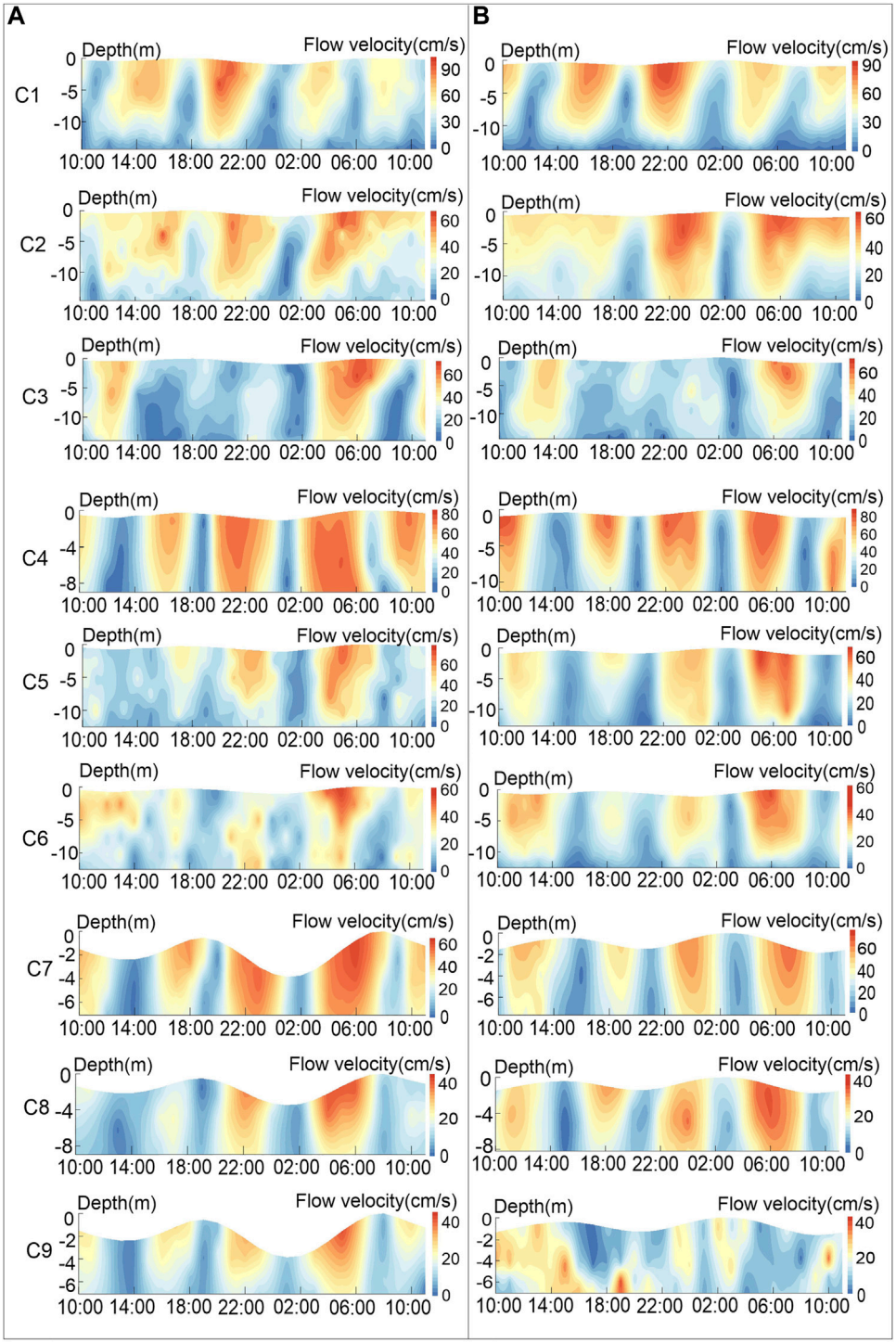

FIGURE 6
Flow velocity profiles at various stations for the spring **(A)** and moderate **(B)** tides.

difference between the surface and bottom was intensified, promoting water stratification. During the moderate tide, water column stratification was weaker than that of spring tide, substantially. According to Eq. 1, the temperature gradient, salinity gradient, and water depth were proportional to the stratification degree and inversely

TABLE 1 Residual current at each station in the spring and moderate tides (velocity: cm/s, direction: degrees).

Tide	Station	Surface		Bottom	
		Velocity	Direction	Velocity	Direction
Spring tide	C1	4.4	201.0	2.7	233.6
	C2	3.3	82.7	1.7	114.0
	C3	8.3	91.0	2.4	275.4
	C4	7.0	127.5	9.0	165.9
	C5	5.6	100.8	0.5	151.0
	C6	3.9	43.0	2.0	267.6
	C7	1.5	46.4	1.2	180.5
	C8	2.7	53.2	2.0	129.4
	C9	2.5	69.4	2.4	115.6
Moderate tide	C1	3.6	66.7	0.6	230.4
	C2	4.8	91.5	0.8	234.3
	C3	6.8	82.3	4.7	191.2
	C4	4.9	130.1	4.9	194.1
	C5	3.3	16.5	2.5	237.9
	C6	3.2	168.6	2.6	244.9
	C7	3.8	17.4	0.2	231.1
	C8	2.6	63.7	2.4	162.6
	C9	1.9	155.3	2.1	137.0

proportional to the flow velocity gradient. Among them, the average water depth of the spring and the moderate tide was not much different (difference value was less than 0.5 m), and the flow velocity gradient during the spring tide was stronger than that of the moderate tide. In addition, during the short period between spring and moderate tides, the salinity gradient did not change much (Figures 7D,H). According to the Global Weather Network (www.tianqi.com), the average air temperature in Laizhou Bay in April and May 2020 was 13.0 and 19.5°C, respectively. In addition, Figures 7B,F showed that the water temperature difference value (1.2 °C) of the spring tide was larger than that of the moderate tide (0.7°C). Thus, the water temperature was the main cause of high stratification degree. Moreover, Q also decreased substantially during the moderate tide (Figures 9A–D). From the analysis of horizontal distribution, the stratification degree at the C5 station in the middle of Laizhou Bay was the most considerable, which may be related to the substantial depth and low flow velocity, which was conducive to stratification. However, due to shallow water depth and tidal waves deformation in coastal waters, water column stratification could not be easily established.

This study utilized the vertical gradient method for expression to further analyze the depth at which thermocline occurred (Jiang et al., 2016). According to that method, the water column with a temperature gradient greater than or equal to 0.2 C/m in shallow water (depth of less than 200 m) is defined as thermocline. The upper limit depth is the depth of the upper water column reaching the critical value of the temperature gradient, and the lower limit depth is the depth of the lower water column. In this study, typical C3–C5, and C9 stations were selected for simultaneous analysis (April and May 2020, 14:00), and the results are shown in Figures 8C, D, G, H and Figures 9C, D, G, H. The thermocline thickness varied between 2.0 and 4.5 m and the depth of the lower thermocline was about 2.0–4.5 m.

4.5 Suspended sediment flux

The suspended sediment fluxes (F) at each station were calculated for the spring and moderate tides (Table 2). The suspended sediment flux of the spring and moderate tides at each station ranged from 0.57 to 9.38 $g\,s^{-1}{\cdot}m^{-1}$ and 1.30–13.62 $g\,s^{-1}{\cdot}m^{-1}$, respectively. Furthermore, the F of these stations were oriented towards land. The direction of the highest suspended sediment flux was 184.41° during the moderate tide at the C4 station, and the direction of the minimum suspended sediment flux was 171.64° in spring tide

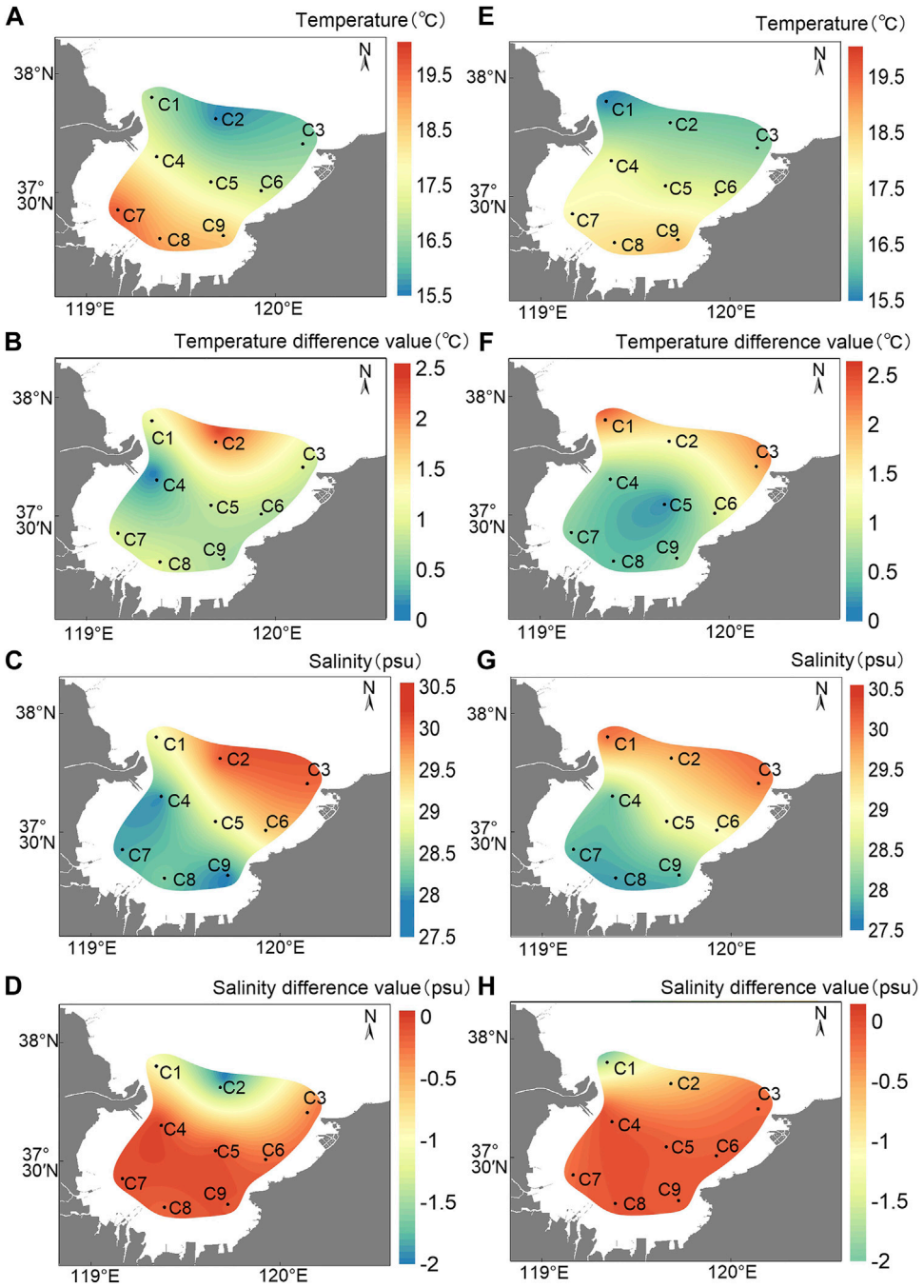

FIGURE 7
Contour of average temperature **(A)** and salinity **(C)** during the spring tide; surface minus bottom temperature **(B)** and salinity **(D)** difference during the spring tide; contour of average temperature **(E)** and salinity **(G)** during the moderate tide; surface minus bottom temperature **(F)** and salinity **(H)** difference during the moderate tide.

at the C8 station. The flux of suspended sediment transport generated by $T_6 + T_7 + T_8$ accounted for an average of only 1.73% of suspended sediment flux, therefore its contribution to the suspended sediment flux was negligible. $T_1 + T_2$ were the dominant elements (the average ratio of $T_1 + T_2$ to F reaches 1.01), and $T_3 + T_4 + T_5$ increased their proportion from the bay mouth to the head of the bay. During moderate tide (Table 2), average suspended sediment flux

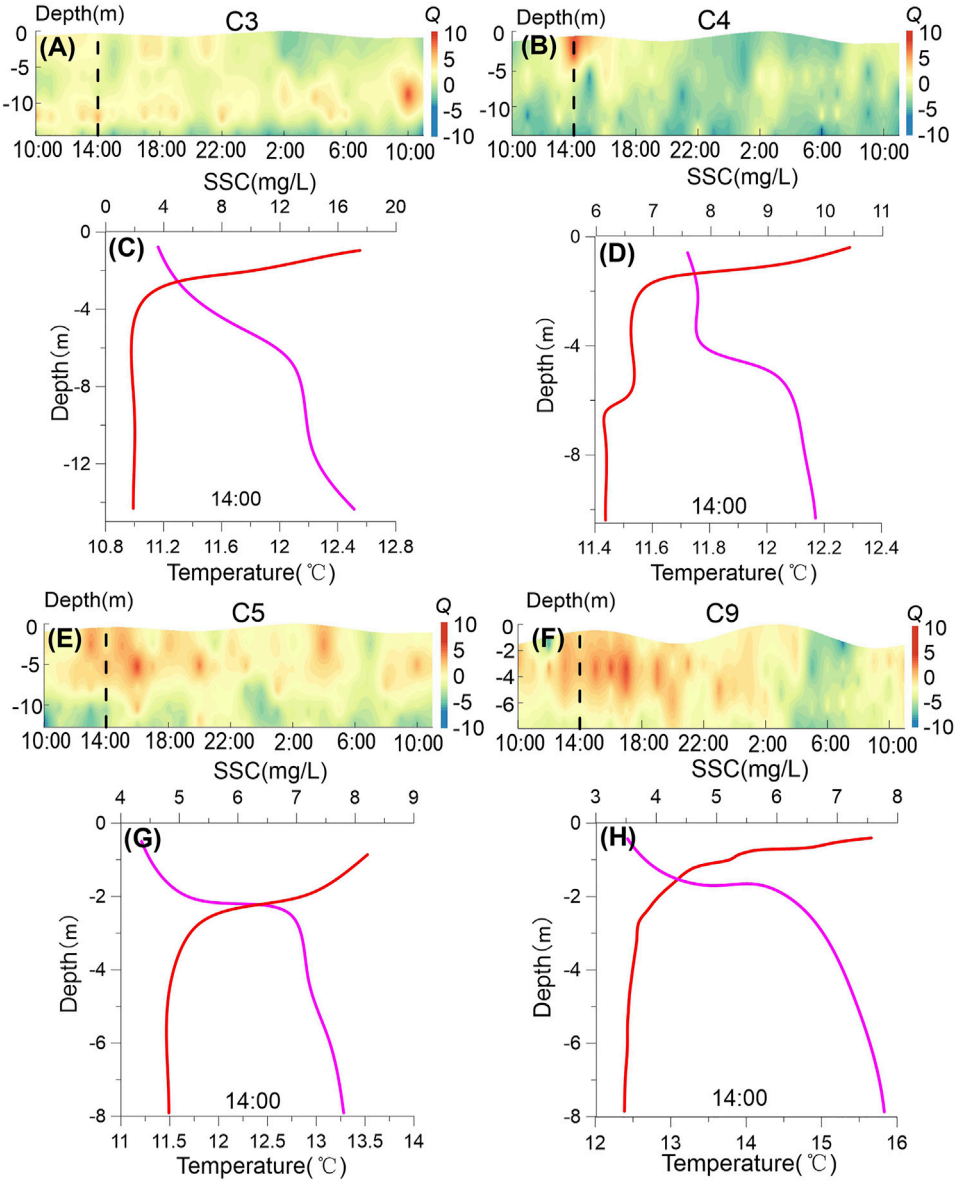

FIGURE 8
The time series diagrams of Q (Q = ln (Rig/0.25)) during the spring tide **(A,B,E,F)**, the vertical sections of temperature (red line) and SSC (fuchsia line) at typical stations at 14:00 in May 2020 **(C,D,G,H)**.

of moderate tide (4.15 g s^{-1} m^{-1}) was higher to those of the spring tide (3.87 g s^{-1} m^{-1}). Overall, according to the results of Table 2, the transport items of T_1, T_2, and $T_3 + T_4 + T_5$ constitute the main part of the suspended sediment flux in Laizhou Bay, accounting for 0.68–1.49, 0.02–0.65, 0.01–0.54 respectively with F, of which T_1 is the main transport term. The suspended sediment flux generated in western Laizhou Bay was considerably higher, followed by that in the middle of Laizhou Bay, and was lowest in eastern Laizhou Bay (except for the C9 station). The Lagrange transport term ($T_1 + T_2$) had the highest proportion and played the most important function, followed by the tidal pumping transport term ($T_3 + T_4 + T_5$).

5 Discussion

5.1 Controlling factors of SSC variations

SSC is influenced by many factors related to runoff, seabed sediment, tide, tidal current, wave, and wind-ocean current (Guo et al., 2017; Qiu et al., 2017; Bo Liu et al., 2020). In

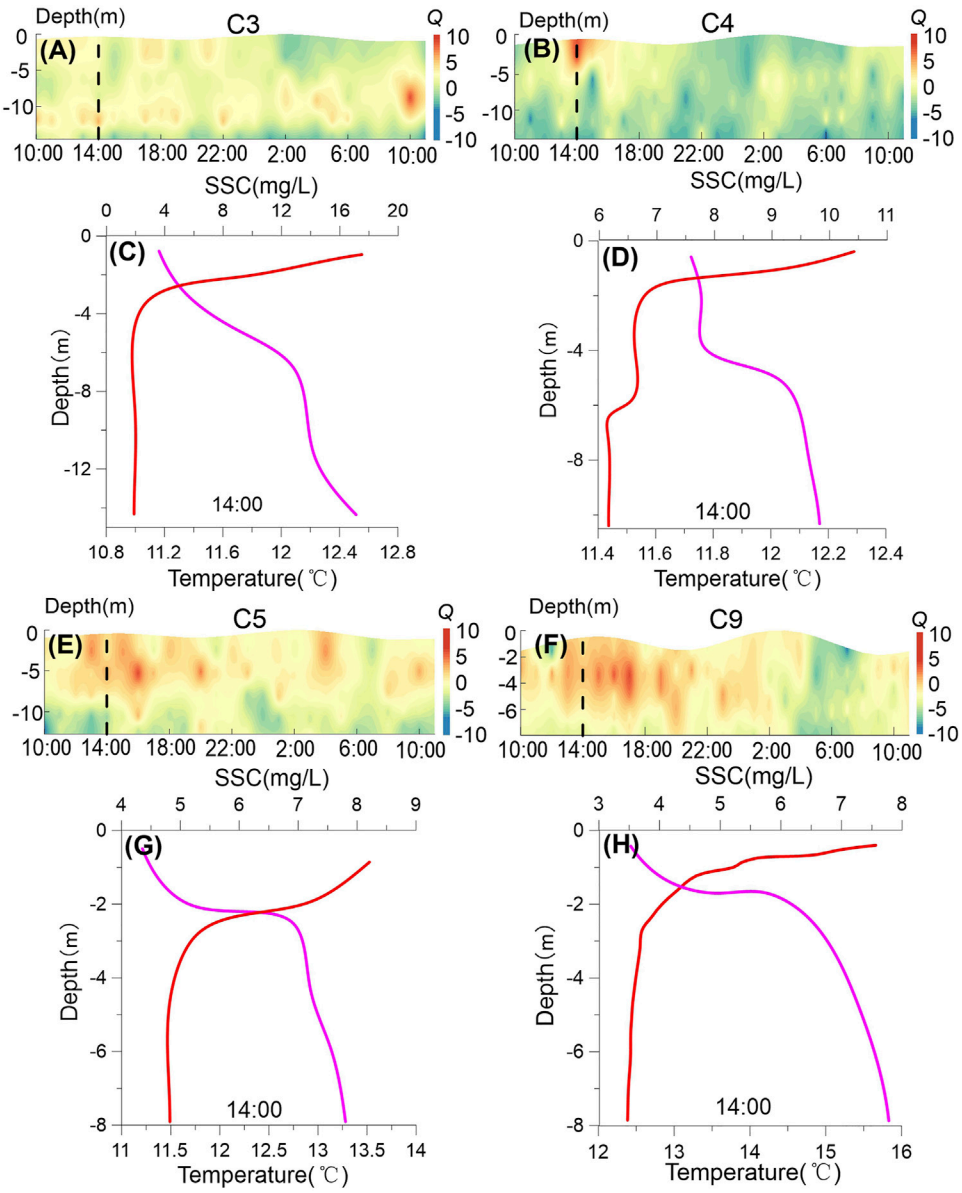

FIGURE 9
The time series diagrams of *Q* (*Q* = ln (*Rig*/0.25)) during the moderate tide **(A,B,E,F)**, the vertical sections of temperature (red line) and SSC (fuchsia line) at 14:00 in April 2020 **(C,D,G,H)**.

addition, the inflow of the material of the Yellow River brings complicated changes to the study of suspended sediment transport in Laizhou Bay. Not only do sediment particles and colloids from the Yellow River (Hill et al., 2009; Geyer and Maccready, 2014) have an important impact on deposition and transport of suspended sediment in Laizhou Bay, but the inflow of a large amount of diluted water into the bay would affect water density and circulation of Laizhou Bay, thereby changing the water structure (Leblond et al., 1986). We will discuss the primary controlling factors of SSC and suspended sediment transport mechanisms in Laizhou Bay from the following perspectives.

5.1.1 Influences of tidal current on the SSC

Under normal weather and tidal conditions, tidal current is an important dynamic source of suspended sediment transport in a semi-enclosed sea (Du et al., 2012; Bo Liu et al., 2020). We analyzed and described the relationship between flow velocity

TABLE 2 The sediment transport flux at various stations during the spring and moderate tides (items without parentheses are sediment transport flux ($g \cdot s^{-1} \cdot m^{-1}$), and items in parentheses are suspended sediment transport direction (degrees)).

Tide	Station	T_1	T_2	$T_1 + T_2$	$T_3 + T_4 + T_5$	$T_6 + T_7 + T_8$	F
Spring tide	C1	8.59	0.37	8.75	1.39	0.04	7.72
		(225.67)	(161.1)	(203.48)	(344.96)	(330.71)	(210.25)
	C2	8.18	0.16	8.2	1.05	0.02	7.61
		(237.23)	(155.06)	(236.11)	(10.23)	(239.61)	(242.49)
	C3	0.85	0.06	0.82	0.24	0.02	0.57
		(159.54)	(40.25)	(155.75)	(6.05)	(205.57)	(217.04)
	C4	10.78	0.59	10.42	2.12	0.13	9.38
		(143.45)	(14.89)	(140.92)	(31.35)	(180.43)	(129.97)
	C5	0.47	0.1	0.41	0.06	0.02	0.38
		(173.44)	(44.61)	(162.69)	(304.87)	(196.03)	(171.64)
	C6	0.66	0.26	0.54	0.13	0.01	0.59
		(265.43)	(63.19)	(217.75)	(211.18)	(168.61)	(214.84)
	C7	1.41	2.25	2.15	1.87	0.03	3.45
		(252.07)	(139.58)	(176.98)	(115.13)	(280.64)	(149.49)
	C8	0.53	0.19	0.53	0.34	0.06	0.89
		(160.77)	(62.6)	(140.3)	(144.68)	(240.93)	(147.73)
	C9	5.19	0.22	4.98	0.55	0.19	4.66
		(155.65)	(339.12)	(155.5)	(351.68)	(192.54)	(153.51)
Moderate tide	C1	9.05	0.76	8.46	0.94	0.08	7.54
		(196.74)	(339.09)	(199.88)	(345.78)	(349.02)	(202.81)
	C2	3.03	0.15	3.05	0.13	0.01	2.95
		(158.92)	(242.39)	(161.72)	(288.88)	(3.01)	(163.41)
	C3	2.11	0.24	2.21	1.07	0.04	2.34
		(152.7)	(222.53)	(158.48)	(252.26)	(10.99)	(184.99)
	C4	14.97	0.58	14.42	0.92	0.02	13.62
		(183.27)	(19.23)	(182.64)	(335.26)	(130.69)	(184.41)
	C5	0.88	0.2	1.08	0.25	0.01	1.30
		(243.7)	(241.21)	(243.24)	(213.16)	(36.99)	(237.65)
	C6	0.80	0.14	0.89	0.06	0.01	0.94
		(266.17)	(353.45)	(253.64)	(208.87)	(180.73)	(219.08)
	C7	3.02	2.02	5.00	0.58	0.05	4.43
		(131.67)	(117.85)	(126.14)	(165.28)	(158.04)	(124.58)
	C8	0.74	0.04	0.75	0.02	0.00	0.73
		(169.77)	(254.23)	(172.68)	(40.04)	(29.33)	(172.02)
	C9	3.19	0.44	3.62	0.04	0.02	3.58
		(237.47)	(227.2)	(236.22)	(48.66)	(335.08)	(236.64)

and SSC at the following nine stations (C1–C9) in spring and moderate tides, as shown in Figures 4, 6, respectively. Theoretically, there were two important sources of suspended sediment for a given station, local resuspension and advection transportation (Yu et al., 2012; Xiong et al., 2017). The horizontal advection of the SSC gradient resulted in SSC tidal variations (Ni et al., 2014). It is known that the combined effects of suspended sediment particle size and tidal current can cause sediment resuspension time lag on the inland shelf and influence cross-shore SSC distribution (Niedoroda et al., 1995; Guillén et al., 2002). In addition, as seen in Figure 3E, coarse-grained Yellow River sediment was rapidly deposited near the Yellow River delta, while fine-grained sediment was transported to the southern and northern Yellow River mouth, influenced by the isobaric-parallel tidal current (Qiao et al., 2010). As seen in Figures 3A,C, 4, the distribution of the surface SSC corresponded well with the tidal

current field. Through remote sensing images, Li et al. (2001) found that the current field and distribution of suspended sediment in the Yellow River mouth was controlled by the interaction between the river and the tidal current, rather than by waves. Similarly, Chao Jiang et al. (2017) and Bo Liu et al. (2020) observed this characteristic in southwestern and northeastern Laizhou Bay.

As the main current movement in the Bohai Sea, tidal current is the main driving force of sediment transport in Laizhou Bay (Qin et al., 1985). There were strong and weak tidal current fields in Laizhou Bay. The high-velocity field was located outside the Yellow River mouth and the weak-velocity field was located in southeast Laizhou Bay (Figure 5). The flow velocity was the highest outside the Yellow River mouth, and showed a tongue-like decreasing trend to the north and south. The velocity decreases rapidly towards the mouth (Figure 5). High surface SSC in Laizhou Bay mainly existed in the spatial velocity the high-velocity field, and surface SSC decreased as the flow velocity decreased. The suspended sediment from the Yellow River mouth firstly diffused southward and southeastward (towards the head of Laizhou Bay). However, the influence scope of suspended sediment is generally located in the shallow coastal sea withing isobaths of about 15 m (Figure 3). The existence of the high-velocity field controlled the outer boundary of the diffusion of suspended sediment into Laizhou Bay. The SSC in the middle and eastern Laizhou Bay was relatively low. Therefore, there was a strong correspondence between the high SSC zone in Laizhou Bay and the high-velocity field outside the Yellow River mouth (Figures 3, 5). The diffusion of such surface suspended sediment in Laizhou Bay is roughly consistent with the distribution of low-salt sea area near the Yellow River mouth (Figures 3A,C, 7C,G). In addition, not only the formation of the low SSC field in eastern Laizhou Bay corresponds to the weak tidal current (Figures 3, 5), but may be also related to the lack of suspended sediment sources (Chen et al., 2015).

Aside from advection transport, another factor that contributed to SSC variation was local resuspension. In addition to the sediment types, external variables such as waves and tidal currents also had an impact on the local resuspension (Sarik and Charitha, 2020). Near-bed turbulence was the primary factor affecting sediment resuspension in calm weather conditions as well as sediment characteristics (particle size, etc.), and was very common in estuarine and coastal environments (Fettweis et al., 2006; Jiang et al., 2020). The sediment lifting of the tidal current was controlled by the diffusion of the turbulence, which relates to its flow velocity, motion viscosity coefficient of the water column, and the roughness of the seabed. The SSC varied periodically due to the alternation of the flood and ebb tides and the fluctuating flow velocity. Although the flow velocity also increased, it did not reach the peak value rapidly or correspondingly, but lagged behind the peak of the flow velocity (Figures 4, 6). Rather, the resuspension and diffusion of suspended sediment required a time process. The lag time varied according to the different sea areas and seasons (Yuan et al., 2011), which is consistent with previous research on bays and shallow seas (Rui Jiang et al., 2017; Bo Liu et al., 2020; Meng et al., 2020).

Notably, not all the flow velocity peak produced the SSC peak, which suggests that under the same conditions, the bottom flow velocity was critical for sediment resuspension (Scully and Friedrichs, 2003). For example, the C5 station reached the peak of surface flow velocity at approximately 16:00 (Figure 6A), but the bottom flow velocity did not increase considerably, resulting in no considerable increase of SSC (Figure 4E). At approximately 05:00, the bottom flow velocity increased considerably, which resulted in high SSC. It can be considered that tidal current not only influenced horizontal distribution of SSC, but influenced vertical distribution of SSC.

5.1.2 Relationship between water stratification and SSC

Water mixing affects not only the tidal current field, but is also closely related to the vertical diffusion of SSC (Li et al., 2013b; Li, 2018; Tong et al., 2018; Yang et al., 2021; Li et al., 2022). In this study, water column stratification hindered the vertical diffusion of suspended sediment. Figures 5, 6 show that the bottom SSC at the C3, C4, and C5 stations were much higher than surface SSC, mainly because seabed sediment had entered the water column. Since the degree of diffusion was inhibited by the stratification, the suspended sediment could not spread effectively in the vertical direction, resulting in a large difference in the surface and bottom SSC. Bi et al. (2010) studied sediment transport into the Yellow River in the summer and winter, and found that the water column was highly stratified in the summer, and that the gradient of vertical SSC was considerable, which is consistent with our observations. In windy weather conditions during the winter, the stratification of the water column was broken, and the surface SSC was similar to the bottom (Bi et al., 2021).

In addition, Scully and Friedrichs (2003) discovered that sediment resuspension in the substrate depended on the critical shear stress, which was less affected by lamination. However, after the sediment entered the water column, its resuspension height and duration in the water column were determined by the turbulence diffusion coefficient at this depth, which was greatly impacted by lamination. The degree of influence was inversely proportional to the stratification height from the seafloor, which was proportional to stratification strength (Scully and Friedrichs, 2003; Courtney et al., 2022). According to Figure 6A, during the spring tide at 19:30–22:00 (from low tide to high tide), although the highest near-bed flow velocity exceeded 40 cm/s at flood tide, the SSC did not increase considerably. The bottom SSC reached a peak rapidly only at the time of rest (22:00) when the strength of stratification was the weakest (Q less than 0). Although we are

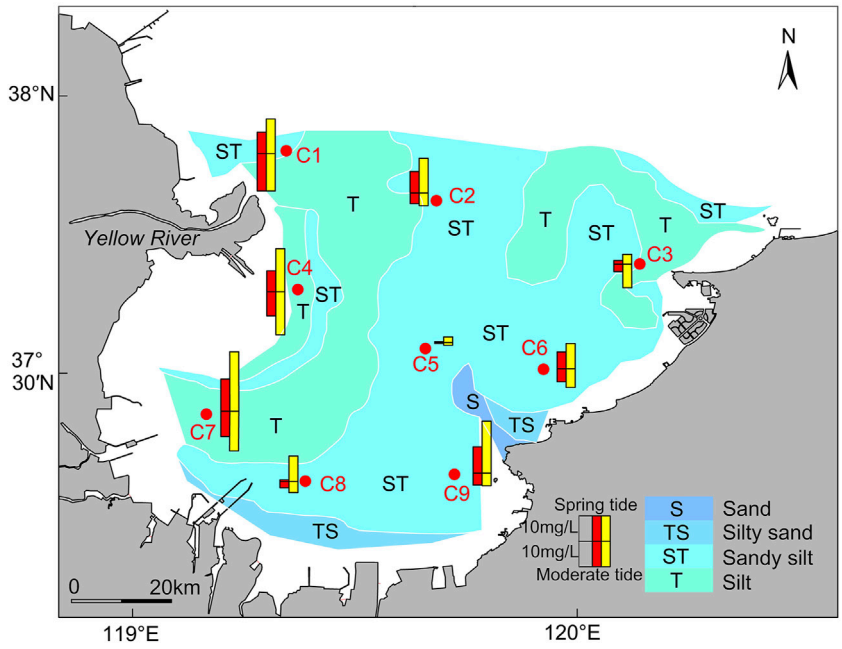

FIGURE 10
Distribution of seabed sediment types (adapted from Qiao et al. (2010)) and distribution of the surface (red rectangle) and bottom SSC (yellow rectangle).

not directly observing near-bed turbulence, the study shown that water column stratification inhibited the intensity of turbulent mixing near the bottom layer (Scully and Friedrichs, 2003; Yuan et al., 2011). When the stratification weakened, water turbulence diffusion strengthened, and the sediment rapidly diffused to a higher elevation. Most Q was less than 0 (except for around 14: 00) at the C4 station (Figures 8D, 9D) in particular, indicating that vertical mixing was dominant during this period. Furthermore, the difference between surface and bottom SSC also decreased, and suspended sediment particles could be effectively diffused vertically.

Moreover, water mixing plays the important role for vertical diffusion of suspended sediment and local resuspension by influencing the turbulence efficiency. When stratification exists in the water column, turbulence is inhibited by that stratification. Sediment resuspension is largely controlled by near-bed turbulence (Ali and Dey, 2016). By observing the flow velocity variations at the C5 station around 04:00–06:00 (flood tide) during the spring tide (Figure 6A), we found that when the near-bottom flow velocity gradually increased at 04:00, the bottom SSC rose suddenly at about 05:00. Although both the bottom flow velocity and the corresponding SSC began to decrease after that, the surface flow velocity reached a maximum value at around 05:30. This suggested that when the bottom flow velocity increased, the seabed sediment resuspended and formed a high SSC zone in the bottom layer, and a large vertical SSC gradient formed in the water column. As shown in Figure 8E, the Q value at the C5 station decreased around 05:30–06:00, indicating that the degree of stratification was decreasing. The continuous vertical diffusion of suspended sediment to the surface water column over time could also verify that the degree of stratification weakened at 05:30–06:00 at the C5 station. In general, tidal current is the main driving force for sediment resuspension under normal weather. In other words, water column stratification reduced the sediment resuspension by inhibiting near-bed turbulence, and then affected vertical SSC.

In summary, water column stratification influenced the vertical SSC variation by hindering the vertical diffusion of suspended sediment and affecting the sediment resuspension, thereby forming a layer with high SSC at the bottom (Stretch et al., 2010). In addition, under normal weather, the weak stratification during moderate tidal was explained why, in normal weather, the average SSC of the middle tide was higher than that of the spring tide, even though flow velocity during spring tide was higher than that of moderate tide (Figure 3).

5.1.3 Effect of seabed sediment on distribution of suspended sediment

The seabed sediment types also have a considerable influence on the distribution characteristics of SSC, mainly because fine-grained sediment is one of the important components of suspended sediment in water column (Qiao et al., 2010; Wang

et al., 2020). In addition, seabed sediment was a key element in the formation of resuspension. Many recent studies have focused on the effect of resuspension on suspended sediment transport, particularly in explaining seasonal sediment transport patterns in the Bohai, Yellow, and East China Seas (Gong et al., 2021). Thus, the analysis of seabed sediment types was one of the major methods for studying the suspended sediment distribution in Laizhou Bay. Wang and Wang (2005) found that the high turbidity zone around the Yellow River mouth was closely related to the types of seabed sediment in Laizhou Bay, as shown in Figures 3, 10. Furthermore, monsoon and wave action have been found to play an important role in seabed sediment resuspension in the Bohai Sea (Qin et al., 1985; Qiao et al., 2010; Bi et al., 2021). However, a more complete explanation of the resuspension process necessitates a closer study during calmer weather.

Laizhou Bay can be divided into four regions based on the spatial distribution of seabed sediment types: western, eastern, central, and southern. The western section was primarily silty sand, whereas the central section was mostly coarse silty sand. The Yellow River continues to be the primary source of sediment (Bi et al., 2010; Qiao et al., 2010). Furthermore, under the influence of tidal currents and waves, the original abandoned QSG delta changed from a sedimentary state to an erosion state and has evolved into a new sediment source (Bi et al., 2021). In addition, since the artificial implementation of water and sediment diversion, the sediment supply of the Yellow River has decreased substantially (Wang et al., 2017). To regulate the balance of water and sediment supply, the sediment of the lower reaches was naturally eroded (Bi et al., 2014). The seabed sediments found in the eastern and southern Laizhou Bay were mostly sandy silt. The primary source of sediment is coastal rivers (Liu et al., 2013; Chen et al., 2015). Furthermore, from the analysis of shoreline changes, the average shoreline erosion rate reached 3.92 m/year during 2006–2013 (Zhan et al., 2017). Thus, coastal erosion is also an important source of sediment in eastern and southern Laizhou Bay, whereas sediment sources tend to be complex and varied in the middle of Laizhou Bay (Qiao et al., 2010; Wang et al., 2010). Because of the weak hydrodynamics (Figures 5, 6) and the low influence by sediment from surrounding rivers and land the middle of Laizhou Bay, the seabed sediment type mainly is silty.

Seabed sediment at the C1 and C4 stations was mostly fine-grained silt or clay silt from the Yellow River, which was prone to resuspension (Wang and Wang, 2005; Zheng et al., 2015). At the C2 station, the seabed sediment type located in the middle and southern Laizhou Bay was mainly coarse silt, and the average flow velocity of the tidal current was relatively slow (28.45 cm/s) (Figure 6), corresponding to the low SSC zone (Figure 4). Combined with the variation characteristic of SSC mentioned above, the bottom sediment resuspension caused by tidal current played an important role for SSC in the water column. However, the proportion of sediment entering the water column under the influence of resuspension is unknown (Qiao et al., 2010). The sediment induced was resuspended and entered the water column as the flow velocity increased and the seabed sediment reached critical shear stress (Chen et al., 2015). Under the influence of water column stratification, suspended sediment cannot be effectively diffused vertically and the high value zone appeared about 1–2 h after peaks of flow velocity sharply. Following that, the flow velocity gradually decreased, resulting in the deposition of suspended sediment. The low SSC value zone developed approximately 2 h after the flood and ebb tides (Figure 5).

The seabed sediment types, strong tidal current zone, and high SSC zone exhibited a strong corresponding relationship in Laizhou Bay (Figures 3–5, 10). Previous studies suggested that under extreme storm surge weather, the maximum SSC in the southwest coastal area of Laizhou Bay may be increased tenfold (Liu et al., 2013). These results indicate that sediment resuspension is very important to the contribution of suspended sediment in Laizhou Bay. Moreover, the grain size of seabed sediment has been found to have a positive effect on resuspension (Wang and Wang, 2005). Under the same dynamic conditions, the seabed sediment (not including clay) with fine particles is more likely to be resuspended. However, the specific linking mechanism between seabed sediment and SSC in Laizhou Bay has remained unclear, as did the resuspension flux.

In order to specifically analyze the behavior of fine-grained sediment in different seabed sediment types, we further studied the sediment resuspension and deposition fluxes. According to the data, the median grain size (D_{50}) of seabed sediment in Laizhou Bay ranged from 0.12 to 0.77 mm (D_{50} of the C3, C6, C8, and C9 stations is from Zhao et al. (2021)). Empirical formulas proposed by Partheniades (1965) and Krone (1962) were used for the calculations, due to the wave effect being very weak (Wang et al., 2014). Further, due to the short interval between the two field survey phases, the median grain size of seabed sediment in the spring and middle tides remained unchanged. Thus, the changes in the spring and moderate tides were similar, and the sediment resuspension and deposition fluxes were selected for calculation during the spring tide.

$$\frac{\mathrm{d}M_{\mathrm{E}}}{\mathrm{d}t} = E\left(\frac{\tau_0}{\tau_{\mathrm{cr}}} - 1\right) \tag{4}$$

$$\tau_{cr} = g\theta_{cr}(\rho_s - \rho)D_{50} \tag{5}$$

$$\frac{\mathrm{d}M_D}{\mathrm{d}t} = C_b W_s\left(1 - \frac{\tau_0}{\tau_{\mathrm{cr}}}\right) \tag{6}$$

In these equations, M_E is the resuspension flux, E is the resuspension constant, τ_0 is the bottom shear stress, τ_{cr} is the critical shear stress, g is the acceleration of gravity, θ_{cr} is the Shields parameter, ρ_s is the sediment density (constant value of 2,650 kg/m^3), ρ is the water column density, D_{50} is the median

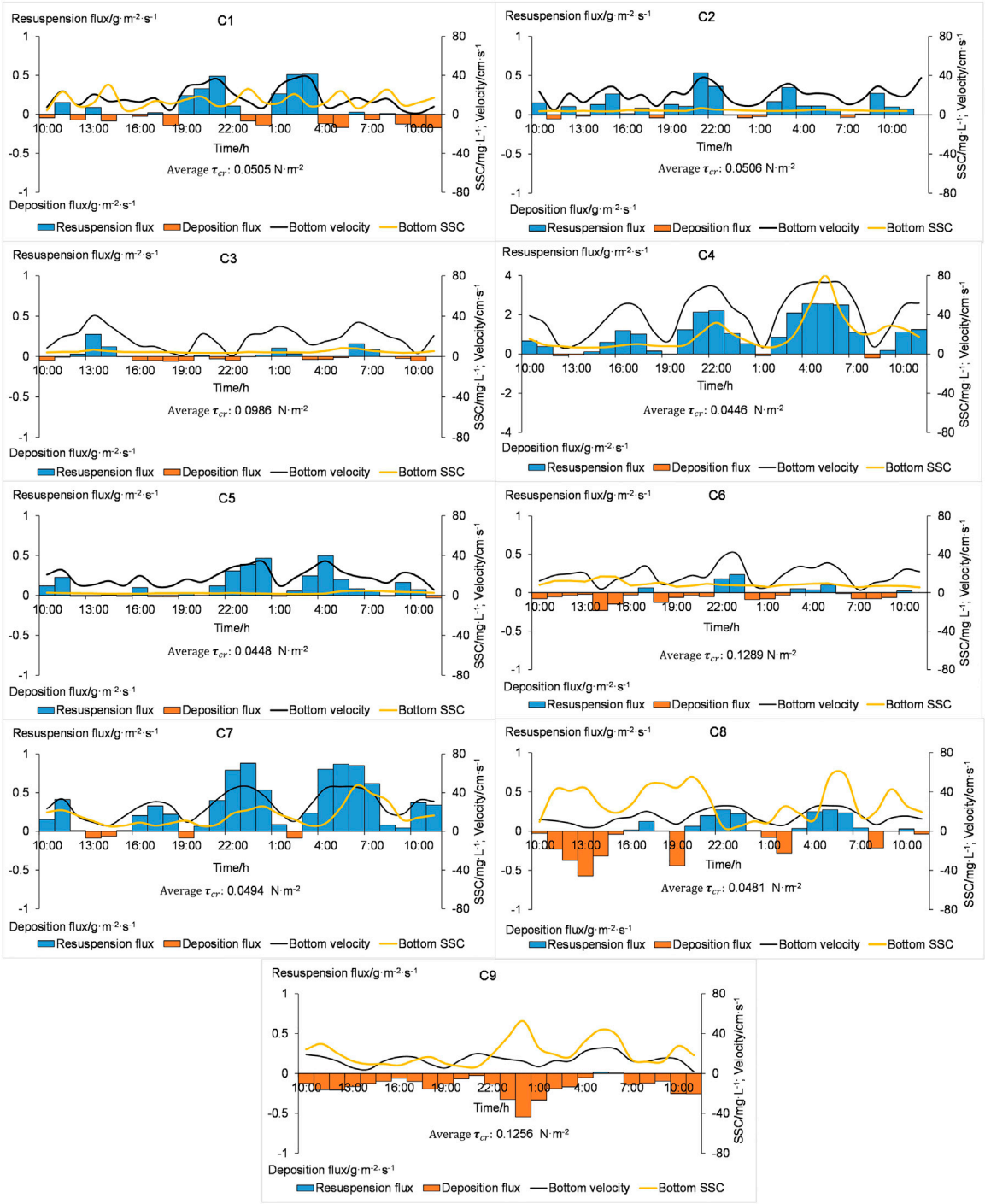

FIGURE 11
Resuspension flux (blue rectangle) and deposition (orange rectangle) flux at each station during the spring tide. Black line represents bottom flow velocity. Yellow line represents bottom SSC.

grain size of seabed sediment, M_D is the deposition fluxes, C_b is the near-bed SSC, and W_s is the settling velocity of suspended sediment.

In this paper, the settling velocity of suspended sediment was calculated using the modified Richardson formula (Huang, 1981):

$$W_s = W_0(1 - 8.9C_v) \quad (7)$$

Where W_0 is the settling velocity of single particle, C_v is the volume ratio of sand content. W_0 is calculated using semi-empirical formula (Camenen, 2007):

$$W_0 = \frac{v}{d}\left[\sqrt{\frac{1}{4}\left(\frac{A}{B}\right)^{2/m} + \left(\frac{4}{3}\frac{d_*}{B}\right)^{1/m}} - \frac{1}{2}\left(\frac{A}{B}\right)^{1/m}\right]^m \quad (8)$$

Where $d*$ is the dimensionless particle diameter; d is the particle diameter; v is the fluid viscosity constant (constant value of $1.007\times10^{-6}ms^2$), A, B, m are the coefficients in the resistance coefficient equation, and their values are based on previous studies (Hu, 2009), which are taken from 38, 3.55, and 1.12, respectively.

The results indicate that there was a large difference in the resuspension flux and deposition flux between various stations in Laizhou Bay (Figure 11), with a variation range of 0.01–2.60 g m^{-2} s^{-1}. Among these, the suspension flux at the C4 station located at the QSG sub-delta lobe was the largest, reaching 2.60 g m^{-2} s^{-1}. In addition to the influence of the elliptic high flow velocity field in the Yellow River mouth (Liu et al., 2005; Qiao et al., 2010), the bottom flow velocity increased, and fine-grained sediment also provided powerful conditions for the occurrence of resuspension. However, the deposition flux at the C4 station was far lower than the resuspension flux, indicating that the fine resuspension sediment particles did not settle *in situ*. Then fine resuspension sediment may be transported to the sea with a slow flow velocity of water, and then deposited. Notably, the resuspension and deposition fluxes at the C1 station near the Yellow River mouth were small (Figure 11). This may be related to the coarsening of grain size near the Yellow River mouth (Bi et al., 2014). Additionally, the water column was stratified due to Yellow River runoff, resulting in substantial differences in surface and bottom flow velocity (Figure 6). Thus, sediment resuspension was not strong at C1 station (Figure 11). Overall, due to the large particle size of seabed sediment in eastern Laizhou Bay, most of the suspended sediment was settled, with the exception of a small quantity of sediment resuspension when the flow velocity approached the flow velocity of initiation of sediment.

The seabed sediment type in the eastern Laizhou Bay was dominated by seasonal river sediment, which was mostly river of mountain stream, with coarse silt as the main sediment entering the sea (Chen et al., 2015). For example, at the C9 station during the spring tide (Figure 11), due to the coarse particle size of seabed sediment (71.95 μm) and low near-bed flow velocity (20.58 cm/s), the critical shear stress generated was not enough to cause sediment resuspension. Thus, there was almost no resuspension flux at C9 station, and the suspended sediments in the water column are basically in a settlement state. This also reflected that the SSC in the water column was not only affected by sediment resuspension, but also advection transport played an important role in maintaining the SSC. In eastern or southern Laizhou Bay, the coarse grain size of seabed sediment and the weak flow velocity were insufficient to produce sediment resuspension when the wave was weak (Figures 5A, 11). However, in western Laizhou Bay, especially near the abandoned QSG delta (C4 station) and southwestern Laizhou Bay (C7 station), the variation of resuspension flux had a strong correspondence with the variation of bottom SSC (Figure 11), indicating that the suspended sediment generated by resuspension may be the main source of the bottom suspended sediment. Therefore, the seabed sediment types are an important factor controlling variation of SSC by influencing resuspension flux.

On this basis, the seabed sediment types had an important control role in the distribution of SSC. The particle size of the seabed sediment would directly affect the strength of the resuspension. The fine-grained seabed sediment was conducive to the generation of resuspension and bottom high SSC. This was critical because the sediment transport occurred primarily through the bottom high SSC layer (Li et al., 2013a; Lu et al., 2018). However, it can also be related to maintaining the suspension duration of fine-grained sediment in the water column to be carried by the tidal current (Hu, 1984; Gao and Jia, 2002).

5.2 Suspended sediment transport mechanisms in Laizhou Bay

Eq. 3 reveals that the net suspended sediment flux is a function of flow velocity, tidal duration, SSC, and depth. Accordingly, the suspended sediment flux is controlled by these factors. The above results indicate that not only did the horizontal and vertical variation of SSC and flow velocity have a great difference, but they also showed asymmetries with tidal duration (Figures 3, 4, 6). There were considerable differences between tidal duration and suspended sediment transport characteristics from other seas, such as Hangzhou Bay, Funing Bay and the south side of the Yangtze River estuary (Wang et al., 2006; Ni et al., 2012; Wang et al., 2014; Meng et al., 2020). Due to the different characteristics of suspended sediment and tidal current in Laizhou Bay, the suspended sediment transport mechanisms were not identical. The suspended sediment transport in western Laizhou Bay was mainly affected by the high-velocity field near the Yellow River mouth. The Yellow River is the second largest sediment-laden river in the world, transporting as much as 1.1 Gt/year of sediment to the ocean (Milliman and Meade, 1983). In addition, the abandoned QSG delta was in a state of severe erosion and had become a new source of sediment (Bi et al., 2021). It has been shown that seabed sediment can re-enter and diffuse into water column under the action of current and waves, combined with the high flow velocity zone near the Yellow River mouth (Figure 5; Liu

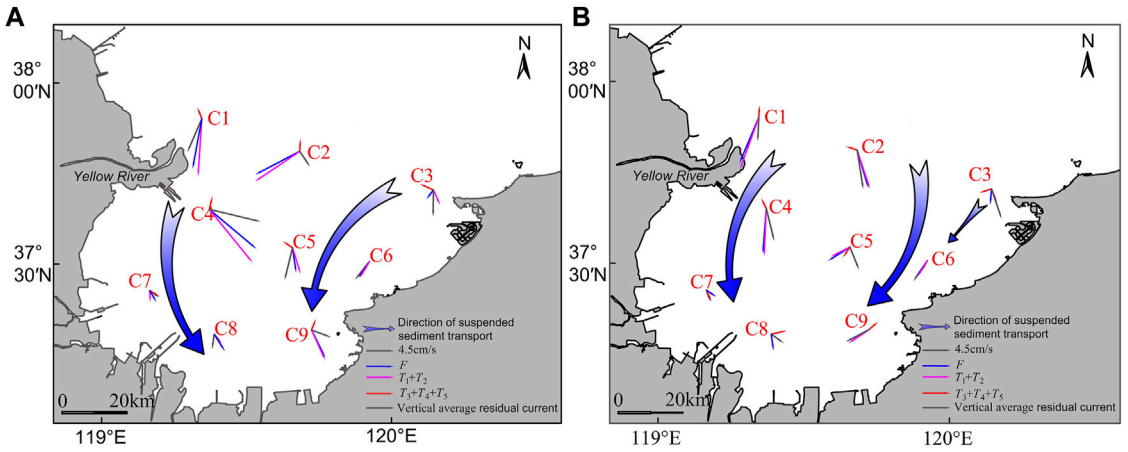

FIGURE 12
Vector diagrams of F (blue arrow), vertical average residual current, $T_1 + T_2$ (gray arrow) and $T_3 + T_4 + T_5$ (red arrow) during the spring **(A)** and moderate **(B)** tides (F of the C6–C8 stations increased to twice the original; $T_3 + T_4 + T_5$ of the C6–C8 stations increased to 6 times the original; and $T_3 + T_4 + T_5$ of the C1–C5 and C9 stations increased to 3 times of original). Gradient blue arrow represents the direction of suspended sediment transport.

et al., 2013), the combined factors of which lead to relatively high suspended sediment flux in western Laizhou Bay. Due to the relatively singular source of sediment (Qin et al., 1985; Zhan et al., 2017), the overall net suspended sediment flux in eastern and southern Laizhou Bay was small (Table 2), which was owing to the coarse particle size of seabed sediment and the weak resuspension effect. $T_1 + T_2$ was related to the residual current, and has a linear relationship with the average SSC and water depth of the local tidal period. The high flow velocity field in northwest Laizhou Bay and the influence of the average SSC makes advective sediment transport dominant in Laizhou Bay. In previous studies, researchers studied the suspended sediment transport mechanism in southwestern and eastern Laizhou Bay in autumn and winter, and the results suggested that $T_1 + T_2$ contributed more than 90% to F. The research results were consistent with the research results of our study. However, F was larger than that in our study, which may be due to the production of a large amount of resuspension sediment under the combined action of strong wind, current, and water temperature, which generated a large amount of resuspension (Bi et al., 2010; Liu et al., 2013).

Tidal pumping is one of the important mechanisms for suspended sediment transport (Jay and Smith, 1990), especially in estuaries with tidal asymmetry. The sediment exchange and lag effect at the bottom of the water column caused the SSC at the flood and ebb tide to be asymmetrical and there was a certain phase difference with the duration and flow velocity (Figures 4, 6), so that suspended sediment flux of the flood and ebb tide during the tidal cycle cannot cancel each other, resulting in the net suspended sediment flux. However, from the mouth to the head of the bay, the process of tidal pumping transport showed a different pattern. For example, at spring tide C4 station, there was different correlation between vertical average velocity and vertical average SSC during ebb and flood tides (Figures 4, 6). This meaned that during the ebb tide, flow velocity was faster than that of high tide, resulting in a higher resuspension flux during the ebb tide. Thus, this led to asymmetries in the SSC and leaded to seaward tidal pumping flux. However, as the sediment from the Yellow Sea was transported to the southern Laizhou Bay during flood tide, the landward advection flux was larger. Therefore, the direction of net suspended sediment transport was generally landward (Figure 12). At C7 station located at the head of the bay, the average flow velocity of flood tide (32.46 cm/s) was greater than that of ebb tide (29.08 cm/s), and the SSC of flood tide was higher than that of ebb tide, so the transport direction of tide pumping was consistent with that of flood tide. During the moderate tide, due to the low flow velocity, the sediment resuspension effect is weakened, which is reflected in the resuspension flux (Figure 12). Therefore, the ratio of the average tidal pumping flux to suspended sediment flux during the moderate tide (12.48%) was considerably lower than that of the spring tide (26.50%).

Residual current also has an important impact on sediment transport in the Bohai Sea (Zhao et al., 1995). The residual current can indicate the direction of suspended sediment transport to some extent (Chen et al., 2015). Generally, in the sea area dominated by the power of the tidal current, the direction of water movement is similar to that of suspended sediment transportation. Thus, residual current direction can basically indicate the net suspended sediment transport direction (Zhao et al., 1995; Bo Liu et al., 2020). Notably, the directions of residual current and suspended sediment transport at some

stations were quite different (Figure 12). In Laizhou Bay, current is more affected by wind (Su, 2005). In spring, Laizhou Bay has changed from the northerly wind to the weak southerly wind. The surface water column was affected by the southern wind, and the overall net surface water was moved to the sea, while net bottom water was carried to the land (Table 1). Further, the activity of bottom water is also a key factor affecting suspended sediment transport (Courtney et al., 2022). This also explains the reason why surface suspended sediment transport was small despite of large residual current value. Thus, the F was moving towards the direction of flood tide (inside the bay). The trend of suspended sediment transport was similar in spring tide and moderate tide. Thus, it is indicated that the tidal-induced residual current controlled the southward transport of suspended sediment when monsoon winds were weak.

In summary, combined with Figure 12, we can obtain the following preliminary understanding: horizontal advection was one of the main transport mechanisms of suspended sediment in Laizhou Bay, followed by tidal pumping. In addition, the result of Q indicates that the overall vertical mixing was weak in spring, and the water column stratification was relatively strong (Figures 8, 9). The suspended sediment transport was mainly caused by advection transport and the re-distribution of resuspension sediment at the bottom under the action of tidal current. The suspended sediment in Laizhou Bay presented a trend of migration from offshore to inland. From the combined analysis of Figures 3, 12, we speculate that the suspended sediment migrated to the bay and was temporarily stored after the long-term movement, deposition, and re-movement cycle under the action of advection and tidal pumping. Under the long and continuous northward gale weather conditions in winter, a large amount of sediment will likely be suspended and transported to eastern Laizhou Bay, possibly through the Bohai Strait (Wang et al., 2011; Bo Liu et al., 2020). Bi et al. (2014) observed that the salinity of winter was lower than that in summer in the southern Bohai Strait, indicating that the diluted water of the Yellow River gathered in Laizhou Bay in spring and summer (this was consistent with our salinity observations), and that winter freshwater was transported along eastern Laizhou Bay by northwesterly winds to the southern Bohai Strait. Overall, it can be concluded that the main transport mechanism of suspended sediment in Laizhou Bay in spring is mainly horizontal advection and tidal pumping. Moreover, the tidal pumping during the spring tide was stronger than that during the moderate tide, as determined from the flow velocity, temperature, and SSC asymmetry between the flood and ebb tides. The tidal and residual current were the main driving forces for the transport of suspended sediment.

Although this study took into account the impact of various factors on SSC, there were several flaws that could be corrected in future studies to better depict the interplay between these factors. Although the resuspension flux and deposition flux of Laizhou Bay were calculated in spring, there is no further knowledge of their behavior during winter, when the resuspension effect is strong. Moreover, our study did not explore the effects of waves and monsoons. However, because of the shallow water of Laizhou Bay, the waves have a considerable impact on seabed sediment resuspension. Previous studies have shown the role of waves and monsoon effects on sediment transport patterns (Yang et al., 1992; Bi et al., 2011).

6 Conclusion

Hydrological and sedimentological data were investigated by two field surveys, each of one tidal cycle (25 h), across nine sample stations and four tide stations, conducted in Laizhou Bay during the spring (May 2020) and moderate tides (April 2020). The primary controlling factors and transport mechanisms of suspended sediment were analyzed based on the tidal current variation characteristics, mixing degree of water column, and distribution of seabed sediment types in Laizhou Bay during the spring. Our primary conclusions are as follows:

(1) Laizhou Bay had an irregular semi-diurnal tide which was dominated by recurrent movement. Northwestern Laizhou Bay had a strong current zone, and the head of the bay had a weak current zone. The vertical flow velocity gradually decreased from the surface to the bottom and the average ratio of surface flow velocity to bottom flow velocity is 2.65.
(2) Overall, the horizontal distribution of SSC indicated that a high SSC zone was mainly present in southwestern Laizhou Bay. The SSC high value region mainly appeared at the bottom. The average SSC of the spring tide was higher than that of the moderate tide. The SSC peaked about 1–2 h after the flow velocity peaked.
(3) The tidal current, mixing degree, and seabed sediment types were the dominant factors controlling the distribution of SSC in Laizhou Bay. The periodic tidal current influenced the vertical and upward periodic variation of SSC. The water column stratification was relatively strong, which inhibited the vertical diffusion of suspended sediment and resulted in the difference between surface and bottom SSC. Moreover, the contribution of fine sediment resuspension flux to SSC in western Laizhou Bay was higher than that in other parts of Laizhou Bay.
(4) According to the decomposition of suspended sediment flux, the Lagrange transport flux occupied the largest proportion and played a dominant role, followed by tidal pump transport. From the mouth of the bay to the top of the bay, the tidal pumping flux was transported in the direction of the dominant tide with different dominant tides. The ratio of the average tidal pumping flux to suspended sediment flux during the spring tide

(26.50%) was considerably higher than that of the moderate tide (12.48%).

Data availability statement

The original contributions presented in the study are included in the article/supplementary material, further inquiries can be directed to the corresponding author.

Author contributions

BX: Conceptualization, Investigation, Writing–original draft, Writing–review and editing. RB: Writing–review and editing. DY: Writing–review and editing. LZ: Project administration, Funding acquisition, Conceptualization, Writing–review and editing. RH: Methodology, Writing–review. CW: Investigation, Visualization. TL: Investigation, Visualization. CL: Visualization, Software, Methodology. PL: Methodology, Visualization, Software. All authors have read and agreed to the published version of the manuscript.

Funding

This study was financially supported by the Sub-project of Basic Condition Investigation and Evaluation of Bohai Region in Shandong (402001202000006_001), the National Natural Science Foundation of China (NSFC, No.41776059), and the National Natural Science Foundation of China (Grants, No.42076037).

Acknowledgments

Our deepest gratitude goes to the reviewers for their careful work and thoughtful suggestions that have helped improve this paper substantially. The authors thank the Ocean University of China and the Qingdao Boyan Marine Environment Technology Co. for their assistance with the laboratory analyses. We would like to thank Editage (https://www.editage.cn/) for English language editing.

Conflict of interest

Author WC was employed by Qingdao Boyan Marine Environment Technology Co., China.

The remaining authors declare that the research was conducted in the absence of any commercial or financial relationships that could be construed as a potential conflict of interest.

Publisher's note

References

Ali, Z, S., and Dey, S. (2016). Hydrodynamics of sediment threshold. *Phys. Fluids (1994).* 28, 075103. doi:10.1063/1.4955103

Allen, P. A. (2008). From landscapes into geological history. *Nature* 451, 274–276. doi:10.1038/nature06586

Bi, N., Yang, Z., Wang, H., Fan, D., and Ji, Y. (2010). Dispersal characteristics of the Huanghe (Yellow River) water and sediment to the sea during Water-Sediment Regulation period of the Huanghe and its dynamic mechanism. *Mar. Geol. Qua. Geol.* 30 (2), 27–34. doi:10.3724/sp.j.1140.2010.02027

Bi, N., Yang, Z., Wang, H., Fan, D., Sun, X., and Lei, K. (2011). Seasonal variation of suspended-sediment transport through the southern Bohai Strait. *Estuar. Coast. Shelf Sci.* 93, 239–247. doi:10.1016/j.ecss.2011.03.007

Bi, N., Wang, H., and Yang, Z. (2014). Recent changes in the erosion–accretion patterns of the active Huanghe (Yellow River) delta lobe caused by human activities. *Cont. Shelf Res.* 90, 70–78. doi:10.1016/j.csr.2014.02.014

Bi, N., Wang, H., Wu, X., Saito, Y., Xu, C., and Yang, Z. (2021). Phase change in evolution of the modern huanghe (Yellow River) delta: Process, pattern, and mechanisms. *Mar. Geol.* 437, 106516. doi:10.1016/j.margeo.2021.106516

Bianchi, T. S., and Allison, M. A. (2009). Large-river delta-front estuaries as natural "recorders" of global environmental change. *Proc. Natl. Acad. Sci. U. S. A.* 106, 8085–8092. doi:10.1073/pnas.0812878106

Bo Liu, B., Hu, R., Yuan, X., Zhu, L., Jiang, S., Nan, V., et al. (2020). Spatiotemporal distribution pattern and transport mechanism of suspended sediments in Longkou offshore under the action of tidal current. *Mar. Geol. Qua. Geol.* 40 (4), 55–66. doi:10.16562/j.cnki.0256-1492.2019072301

Camenen, B. (2007). Simple and general formula for the settling velocity of particles. *J. Hydraul. Eng.* 133, 229–233. doi:10.1061/(asce)0733-9429(2007)133:2(229)

Chao Jiang, C., Pan, S., and Chen, S. (2017). Recent morphological changes of the Yellow River (Huanghe) submerged delta: Causes and environmental implications. *Geomorphology* 293, 93–107. doi:10.1016/j.geomorph.2017.04.036

Chen, B., Liu, J., and Gao, F. (2015). Suspended sediment transport mechanism in Laizhou Bay. *Adv. Water. Resour.* 26 (5), 857–866. doi:10.14042/j.cnki.32.1309.2015.06.012

Courtney, K. H., Jacob, T. W., Matthew, J. F., and Jessica, M. C. (2022). ADCP observations of currents and suspended sediment in the macrotidal gulf of martaban, Myanmar. *Front. Earth Sci. (Lausanne).* 10, 820326. doi:10.3389/feart.2022.820326

Du, J., Pei, Y., Gao, J., Yu, X., Wang, F., Fan, C., et al. (2012). The suspended sediment transport associated with low flow patterns in shallow waters: A case study from the tianjin subtidal area. *Acta. Oceanol. Sin.* 34, 136–144. doi:10.1007/s11783-011-0280-z

Dyer, B. (1997). Estuaries: A physical introduction. *Geogr. J.* 140, 316. doi:10.2307/1797104

Fang, Y., Fang, G., and Zhang, Q. (2000). Numerical simulation and dynamic study of the wintertime circulation of the Bohai Sea. *Chin. J. Oceanol.* 18, 1–9. doi:10.1007/bf02842535

Fettweis, M., Francken, F., Pison, V., and Van den Eynde, D. (2006). Suspended particulate matter dynamics and aggregate sizes in a high turbidity area. *Mar. Geol.* 235, 63–74. doi:10.1016/j.margeo.2006.10.005

Fu, Y., Chen, S., Ji, H., Fan, Y., and Peng, L. (2021). The modern Yellow River delta in transition: Causes and implications. *Mar. Geol.* 436, 106476. doi:10.1016/j.margeo.2021.106476

Gao, S., and Jia, J. (2002). Modeling suspended sediment distribution in continental shelf upwelling/downwelling settings. *Geo-Mar. Lett.* 22, 218–226. doi:10.1007/s00367-002-0116-8

Geyer, W. R., and Maccready, P. (2014). The estuarine circulation. *Annu. Rev. Fluid Mech.* 46, 175–197. doi:10.1146/annurev-fluid-010313-141302

Gong, Z., Ge, R., Feng, Q., Wei, J., Su, M., Jin, C., et al. (2021). Cohesive forces between sediment particles and its impact on incipient motion of sediment:a review. *Adv. Water. Sci.* 32, 801–812. doi:10.14042/j.cnki.32.1309.2021.05.015

Guillén, J., Jiménez, J. A., Palanques, A., Gracia, V., Puig, P., and Sánchez-Arcilla, A. (2002). Sediment resuspension across a microtidal, low-energy inner shelf. *Cont. Shelf Res.* 22, 305–325. doi:10.1016/s0278-4343(01)00059-0

Guo, K., Zou, T., Jiang, D., Tang, C., and Zhang, H. (2017). Variability of Yellow River turbid plume detected with satellite remote sensing during water-sediment regulation. *Cont. Shelf Res.* 135, 74–85. doi:10.1016/j.csr.2017.01.017

Hill, D. F., Ciavola, S. J., Etherington, L., and Klaar, M. (2009). Estimation of freshwater runoff into Glacier Bay, Alaska and incorporation into a tidal circulation model. *Estuar. Coast. Shelf Sci.* 82, 95–107. doi:10.1016/j.ecss.2008.12.019

Hu, D. (1984). Upwelling and sedimentation dynamics I. The role of upwelling in sedimentation in the huanghai Sea and east China sea-a description OF general features. *Chin. J. Oceanol. Limnol.* 2, 13–19. doi:10.1007/BF02888388

Hu, R. (2009). *Sediment transport and dynamic mechanism in the Zhoushan Archipelago sea area*. [dissertation thesis]. Shandong: Ocean University of China.

Hu, R., Ma, F., Wu, J., Zhang, W., Jiang, S., Xu, Y., et al. (2016). Sediment transport in the nearshore area of Phoenix Island. *J. Ocean. Univ. China* 15, 767–782. doi:10.1007/s11802-016-2967-z

Huang, D., Su, J., and Backhaus, J. O. (1999). Modelling the seasonal thermal stratification and baroclinic circulation in the Bohai Sea. *Cont. Shelf Res.* 47, 1485–1505. doi:10.1016/s0278-4343(99)00026-6

Huang, J. (1981). Experimental study of settling properties of cohesive sediment in still water. *Sediment. Res.* 2, 30–41. doi:10.16239/j.cnki.0468-155x.1981.02.003

Ingram, R. G. (1981). Characteristics of the great whale river plume. *J. Geophys. Res.* 86, 2017–2023. doi:10.1029/jc086ic03p02017

Jay, D. A., and Smith, J. D. (1990). Residual circulation in shallow estuaries. 1. Highly stratified, narrow estuaries. *J. Geophys. Res.* 95, 711–731. doi:10.1029/jc095ic01p00711

Jiang, W., Xin, B., Lou, W., and Lian, R. (2016). Comparisons of three thermocline detection methods. *Mar. Fornt.* 33, 41–49. doi:10.11737/j.issn.1003-0239.20l6.03

Jiang, M., Pang, C., Liu, Z., and Jiang, J. (2020). Sediment resuspension in winter in an exceptional low suspended sediment concentration area off Qinhuangdao in the Bohai Sea. *Estuar. Coast. Shelf Sci.* 245, 106859. doi:10.1016/j.ecss.2020.106859

Jillian, M. M., Samuel, Bentley, J., Zhang, K., Jeffrey, O., Ioannis, Y., et al. (2018). Mississippi River subaqueous delta is entering a stage of retrogradation. *Mar. Geol.* 400, 12–23. doi:10.1016/j.margeo.2018.03.001

Krone, B. R. (1962). *Flume studies of the transport of sediment in estuarial schoaling processes*. Berkeley: Hydraulic Engineering Laboratory and Sanitary Engeering Research Laboratory, University of California.

Leblond, P. H., Emery, W. J., and Nicol, T. A. (1986). A climatic model of runoff-driven coastal circulation. *Estuar. Coast. Shelf Sci.* 23, 59–79. doi:10.1016/0272-7714(86)90085-5

Li, G., Tang, Z., Yue, S., Zhuang, K., and Wei, H. (2001). Sedimentation in the shear front off the Yellow River mouth. *Cont. Shelf Res.* 21, 607–625. doi:10.1016/s0278-4343(00)00097-2

Li, X., Hu, G., and Shi, Z. (2013a). Mixing, stratification and tidal straining in dry season within the north passage of the south branch south channel of the Changjiang River estuary. *Port. Waterw. Engi.* 9, 79–88. doi:10.3969/j.issn.1002-4972.2013.09.018

Li, Y., Lei, Q., Wang, A., Yong, Z., Fang, J., and Jian, C. (2013b). Seasonal variation of water column structure and sediment transport in a mud depo-center off the Zhejiang-Fujian coast in China. *Ocean. Dyn.* 63, 679–690. doi:10.1007/s10236-013-0620-6

Li, S., Wang, H., Zhang, Y., Bi, N., Wu, X., and Hu, B. (2015). Variation in sediment load and grain-size under the influence of Water and Sediment Reguration Scheme (WSRS) of the Huanghe (yellow) river. *Mar. Geol. Front.* 31, 20–27. doi:10.16028/j.1009-2722.2015.07003

Li, Z., Jia, J., Wang, Y., and Zhang, G. (2022). Net suspended sediment transport modulated by multiple flood-ebb asymmetries in the progressive tidal wave dominated and partially stratified Changjiang Estuary. *Mar. Geol.* 443, 106702. doi:10.1016/j.margeo.2021.106702

Li, Z., Ruan, Y., Guo, Z. D., Cong, H., Zhang, K. Y., and Takemura, H. (1990). Function and localization of high and low affinity binding sites to muscarinic receptors in longitudinal and circular smooth muscles of human stomach. *Res. Commun. Chem. Pathol. Pharmacol.* 4, 31–42.

Li, X. (2018). *Suspended Sediment Transport in stratified waters: Field observation and numerical simulation of the Changjiang Estuary*. Shanghai: East. China. Norm. Univ.

Liu, H., and Pan, W. (2007). Numerical simulation of the seasonal variations of the stratification and tidal front in the Bohai Sea. *Adv. Water. Sci.* 3, 398–403. doi:10.3321/j.issn:1001-6791.2007.03.015

Liu, Y., Chen, S., and Li, J. (2005). Patterns of variations in the water and sediment fluxes from the Yellow River to the estuary. *B. Mar. Sci.* 24, 1–8. doi:10.3969/j.issn.1001-6392.2005.06.001

Liu, Y., Huang, H., and Yang, X. (2013). The transportation and deposition of suspended sediment and its dynamic mechanism analysis based on Landsat images in the Laizhou Bay. *Acta. Oceanol. Sin.* 35 (6), 43–53. doi:10.3969/j.issn.0253-4193.201

Lu, J., Jiang, J., Li, A., and Ma, X. (2018). Impact of typhoon chan-hom on the marine environment and sediment dynamics on the inner shelf of the east China sea: *In-situ* seafloor observations. *Mar. Geol.* 406, 72–83. doi:10.1016/j.margeo.2018.09.009

Meng, L., Hu, R., Li, Y., Yuan, X., Zhu, L., and Guo, J. (2020). Transport characteristics of suspended sediment in Funing Bay during spring tide in winte. *Mar. Geol. Quat. Geol.* 40, 61–73. doi:10.16562/j.cnki.0256-1492.2019111801

Millero, F. J., and Poisson, A. (1981). International one-atmosphere equation of state of seawater. *Deep Sea Res. Part A. Oceanogr. Res. Pap.* 28, 625–629. doi:10.1016/0198-0149(81)90122-9

Milliman, J. D., and Meade, R. H. (1983). World-wide delivery of river sediment to the oceans. *J. Geol.* 91, 1–21. doi:10.1086/628741

Ni, Z., Chen, H., Dong, L., Shi, Z., Wang, D., and Zhai, Q. (2012). Measurement and analysis of vertical mixing and stratification within the plume outside the changjiang River estuary. *J. Shanghai. J. Univ.* 46, 1862–1873. doi:10.16183/j.cnki.jsjtu.2012.11.030

Ni, W., Wang, Y., Zhou, X., Zhang, J., and Gao, J. (2014). Sediment dynamics in an offshore tidal channel in the southern Yellow Sea. *Int. J. Sediment Res.* 29, 246–259. doi:10.1016/s1001-6279(14)60040-8

Niedoroda, A. W., Reed, C. W., Swift, D. J. P., Arato, H., and Hoyanagi, K. (1995). Modeling shore-normal large-scale coastal evolution. *Mar. Geol.* 126, 181–199. doi:10.1016/0025-3227(95)98961-7

Nour, H. E., Helal, S. A., and Wahab, M. A. (2022). Contamination and health risk assessment of heavy metals in beach sediments of Red Sea and Gulf of Aqaba, Egypt. *Mar. Pollut. Bull.* 177, 113517. doi:10.1016/j.marpolbul.2022.113517

Oliveira, M. L. S., Dotto., G. L., Pinto., D., Alcindo, N., and Silva., L. F. O. (2021). Nanoparticles as vectors of other contaminants in estuarine suspended sediments: Natural and real conditions. *Mar. Pollut. Bull.* 168, 112429. doi:10.1016/j.marpolbul.2021.112429

Pang, W., Dai, Z., Ge, Z., Li, S., Mei, X., Gu, J., et al. (2019). Near-bed cross-shore suspended sediment transport over a meso-macro tidal beach under varied wave conditions. *Estuar. Coast. Shelf Sci.* 217, 69–80. doi:10.1016/j.ecss.2018.11.007

Partheniades, E. (1965). Erosion and deposition of cohesive soils. *J. Hydr. Div.* 91, 105–139. doi:10.1061/jyceaj.0001165

Qiao, S., Shi, X., Zhu, A., Liu, Y., Bi, N., Fang, X., et al. (2010). Distribution and transport of suspended sediments off the Yellow River (huanghe) mouth and the nearby Bohai Sea. *Estuar. Coast. Shelf Sci.* 86 (3), 337–344. doi:10.1016/j.ecss.2009.07.019

Qin, Y., Zhao, Y., and Zhao, S. (1985). *Geology of the Bohai Sea*. Beijing: Science Press, 1–232.

Qiu, Z. F., Xiao, C., Perrie, W., Sun, D., Wang, S., Shen, H., et al. (2017). Using Landsat 8 data to estimate suspended particulate matter in the Yellow River estuary. *J. Geophys. Res. Oceans* 122, 276–290. doi:10.1002/2016jc012412

Rui Jiang, R., Wu, J., Zhu, L., Hu, R., and Yue, N. (2017). The concentration changes and transport mechanism of suspended sediments in southwestern Laizhou Bay. *Mar. Geo. Front.* 33, 25–32. doi:10.16028/j.1009-2722.2017.09004

Sarik, S., and Charitha, P. (2020). Sediment resuspension due to near-bed turbulent coherent structures in the nearshore. *Cont. Shelf Res.* 194, 104048. doi:10.1016/j.csr.2020.104048

Scully, M. E., and Friedrichs, C. T. (2003). The influence of asymmetries in overlying stratifi-cation on near-bed turbulence and sediment suspension in a partially mixed estuary. *Ocean. Dyn.* 53, 208–219. doi:10.1007/s10236-003-0034-y

Shou, W., Zong, H., and Ding, P. (2016). Numerical study of the circulation influenced by runoff input in the Huanghe (Yellow) River Estuary and adjacent waters in summer. *Acta. Oceanol. Sin.* 38, 1–13. doi:10.3969/j.issn.0253-4193.2016.07.001

Simpson, J. J., and Dickey, T. D. (1981). The relationship between downward irradiance and upper ocean structure. *J. Phys. Oceanogr.* 11, 309–323. doi:10.1175/1520-0485(1981)011<0309:TRBDIA>2.0.CO;2

Stretch, D. D., Rottman, J. W., Venayagamoorthy, S. K., Nomura, K. K., and Rehmann, C. R. (2010). Mixing efficiency in decaying stably stratified turbulence. *Dyn. Atmos. Oceans* 49, 25–36. doi:10.1016/j.dynatmoce.2008.11.002

Su, J. (2005). *China Offshore Hydrology*. Beijing: China Ocean Press.

Syvitski, J., and Milliman, J. (2007). Geology, geography, and humans battle for dominance over the delivery of fluvial sediment to the coastal ocean. *J. Geol.* 115 (1), 1–19. doi:10.1086/509246

Tong, C., Li, L., Meng, Y., and Wang, B. (2018). Analysis of stratification-mixing mechanism during spring tide of dry season in the Modaomen waterway. *Hyd-Sci. Eng.* 1, 48–57. doi:10.16198/.enk.1009-640X.2018.01.008

Trowbridge, J. H. (1992). A simple description of the deepening and structure of a stably stratified flow driven by a surface stress. *J. Geophys. Res.* 97 (C10), 15529–15543. doi:10.1029/92JC01512

Turner, J. S., and Benton, E. R. (1974). Buoyancy effects in fluids. *Phys. Today.* 27, 52–53. doi:10.1063/1.3128495

Uncles, R. J., Elliott, R. C. A., and Weston, S. A. (1985). Dispersion of salt and suspended sediment in a partly mixed estuary. *Estuaries* 8, 256–269. doi:10.2307/1351486

Vonda, J. C., Jennifer, B., Valeria, M., James, J. B., Dianne, T., Malcolm, R. C., et al. (2020). Responses of a common New Zealand coastal sponge to elevated suspended sediments: Indications of resilience. *Mar. Environ. Res.* 155, 104886. doi:10.1016/j.marenvres.2020.104886

Wang, W., and Wang, H. (2005). Distribution of suspended matter and its relationship with sediment particle size in Laizhou Bay. *Chin. J. Oceanol. Limnol.* 36, 97–103. doi:10.3321/j.issn:0029-814X.2005.02.001

Wang, Y., Pan, S., Wang, H. V., Gao, J., Yang, S., Wang, A., et al. (2006). Measurements and analysis of water discharges and suspended sediment fluxes in changjiang estuary. *J. Geogr.* 01, 35–46. doi:10.11821/xb200601004

Wang, H., Yang, Z., Saito, Y., Liu, J. P., Sun, X., and Wang, Y. (2007). Stepwise decreases of the Huanghe (Yellow River) sediment load (1950–2005): Impacts of climate change and human activities. *Glob. Planet. Change.* 57, 331–354. doi:10.1016/j.gloplacha.2007.01.003

Wang, K., Shi, X., Cai, S., Qiao, S., and Jiang, X. (2010). Distribution and provenance of the seabed sediment of the Yellow River mouth and Laizhou Bay deduced from heavy minerals. *Mar. Geol. Quat. Geol.* 30, 1–8. doi:10.3724/SP.J.1140.2010.06001

Wang, H., Han, S., Guo, P., and Li, G. (2011). Transportation of sediment from Yellow River in Bohai Sea due to tidal currents. *J. Sediment. Res.* 1, 51–59. doi:10.16239/j.cnki.0468-155x.2011.01.008

Wang, H., Wang, A., Bi, N., Zeng, X., and Xiao, H. (2014). Seasonal distribution of suspended sediment in the Bohai Sea, China. *Cont. Shelf Res.* 90, 17–32. doi:10.1016/j.csr.2014.03.006

Wang, H., Wu, X., Bi, N., Li, S., Yuan, P., Wang, A., et al. (2017). Impacts of the dam-orientated water-sediment regulation scheme on the lower reaches and delta of the Yellow River (Huanghe): A review. *Glob. Planet. Change* 157, 93–113. doi:10.1016/j.gloplacha.2017.08.005

Wang, Y., Zhang, G., Zhou, S., and Meng, L. (2020). Study on critical shear stress of cohesionless uniform single sediment particle. *J. Sediment. Res.* 1, 1–6. doi:10.16239/j.cnki,0468,155x.2020.01.001

Wu, X., Bi, N., Xu, J., Nittrouer, J. A., Yang, Z., Saito, Y., et al. (2017). Stepwise morphological evolution of the active Yellow River (Huanghe) delta lobe (1976-2013): Dominant roles of riverine discharge and sediment grain size. *Geomorphology* 292, 115–127. doi:10.1016/j.geomorph.2017.04.042

Xingmin Liu, X., Qiao, L., Zhong, Y., Wan, X., Xue, W., and Liu, P. (2020). Pathways of suspended sediments transported from the Yellow River mouth to the Bohai Sea and Yellow Sea. *Estuar. Coast. Shelf Sci.* 236, 106639. doi:10.1016/j.ecss.2020.106639

Xiong, J., Wang, X., Wang, Y., Chen, J., Shi, B., Gao, J., et al. (2017). Mechanisms of maintaining high suspended sediment concentration over tide-dominated offshore shoals in the southern Yellow Sea. *Estuar. Coast. Shelf Sci.* 191, 221–233. doi:10.1016/j.ecss.2017.04.023

Xu, S., and Xu, Y. (2013). Review on water environment evolution and strategy after land reclamation. *Adv. Water. Sci.* 24, 138–145. doi:10.14042/j.cnki.32.1309.2013.01.016

Yang, Z., Guo, Z., Wang, Z., Xu, J., and Gao, W. (1992). Suspended sediments on the yellow and east China sea shelf and macropattern of their being transported to the eastern deeper sea. *Acta. Oceanol. Sin.* 14 (2), 81–90. doi:10.1007/BF02677081

Yang, G., Wang, X., Cheng, Z., Zhong, Y., and Thomas, O. (2021). Modelling study on estuarine circulation and its effect on the turbidity maximum zone in the Yalu River Estuary, China. *Estuar. Coast. Shelf Sci.* 263, 107634. doi:10.1016/j.ecss.2021.107634

Yin, D., Wu, J., Hu, R., and Zhu, L. (2013). Recent evolution and sediment transport patterns of the Dengzhou Shoal. *Mar. Geol. Front.* 29 (8), 25–32. doi:10.16028/j.1009-2722.2013.08.007

Yu, Q., Wang, Y., Flemming, B., and Gao, S. (2012). Tide-induced suspended sediment transport: Depth-averaged concentrations and horizontal residual fluxes. *Cont. Shelf Res.* 34, 53–63. doi:10.1016/j.csr.2011.11.015

Yuan, Y., Wang, W., Gao, H., and Guo, X. (2011). Resuspension and associated horizontal, settling fluxes of sediment in the weakly stratified Laizhou Bay mouth. *Oceanol. Limnol. Sin.* 42, 1–8. doi:10.11693/hyhz201101001001

Zhan, C., Yun, J., Wang, Q., Li, Z., and Zhou, D. (2017). Spatial and temporal dynamics of sandy coastal geomorphology in the east of Laizhou Bay over recent 60 years. *Acta. Oceanol. Sin.* 39, 90–100. doi:10.3969/j.issn.0253-4193.2017.09.009

Zhao, B., Zhuang, G., and Cao, D. (1995). Circulation, tidal residual currents and their effects on the sedimentation in the Bohai sea. *Oceanol. Limnol. Sin.* 26, 466–473. doi:10.3321/jissn:0029-814X.1995.05.003

Zhao, Y., Sun, S., You, L., Su, B., Ma, Y., Li, M., et al. (2020). Distribution characteristics of grain size and heavy metals of sediments in Laizhou Bay. *Mar. Sci.* 45, 43–50. doi:10.11759/hykx20200806004

Zheng, J., Jia, Y., Liu, X., Liu, B., Fu, T., and Zhang, L. (2015). Field measurement of sediment critical shear stress in the modern Yellow River Delta. *Acta. Oceanol. Sin.* 37, 86–98. doi:10.3969/j.issn.0253-4193.215

Zhou, Z., Bian, C., Wang, C., Jiang, W., and Bi, R. (2017). Quantitative assessment on multiple timescale features and dynamics of sea surface suspended sediment concentration using remote sensing data. *J. Geophys. Res. Oceans* 122, 8739–8752. doi:10.1002/2017jc013082